

Hessian Aware Low-Rank Perturbation for Order-Robust Continual Learning

Jiaqi Li, Yuanhao Lai, Rui Wang, Changjian Shui, Sabyasachi Sahoo, Charles X. Ling, Shichun Yang, Boyu Wang, Christian Gagné, Fan Zhou

Abstract—Continual learning aims to learn a series of tasks sequentially without forgetting the knowledge acquired from the previous ones. In this work, we propose the Hessian Aware Low-Rank Perturbation algorithm for continual learning. By modeling the parameter transitions along the sequential tasks with the weight matrix transformation, we propose to apply the low-rank approximation on the task-adaptive parameters in each layer of the neural networks. Specifically, we theoretically demonstrate the quantitative relationship between the Hessian and the proposed low-rank approximation. The approximation ranks are then globally determined according to the marginal increment of the empirical loss estimated by the layer-specific gradient and low-rank approximation error. Furthermore, we control the model capacity by pruning less important parameters to diminish the parameter growth. We conduct extensive experiments on various benchmarks, including a dataset with large-scale tasks, and compare our method against some recent state-of-the-art methods to demonstrate the effectiveness and scalability of our proposed method. Empirical results show that our method performs better on different benchmarks, especially in achieving task order robustness and handling the forgetting issue. The source code is at <https://github.com/lijiaqi/HALRP>.

Index Terms—Non-stationary Environment, Continual Learning, Low-rank Perturbation, Hessian information

1 INTRODUCTION

THE conventional machine learning paradigm assumes all the data are simultaneously accessed and trained. However, in practical scenarios, data are often collected from different tasks and sequentially accessed in a specific order. Continual Learning (CL) aims to gradually learn from novel tasks and preserve valuable knowledge from previous ones. Despite this promising paradigm, CL is usually faced with a dilemma between *memory stability* and *learning plasticity*: when adapting among the dynamic data distributions, it has been shown that the neural networks can easily forget the learned knowledge of previous tasks when facing a new one, which is known as *Catastrophic Forgetting* (CF) [1].

One possible reason for this forgetting issue can be the parameter drift from the previous tasks to the new ones, which is caused by the optimization process with the use of stochastic gradient descent and its variants [2], [3]. To mitigate the obliviousness to past knowledge, some works [4]–[8] proposed to constrain the optimization objective for the knowledge of new tasks with additional penalty regularization terms. These approaches were shown as ineffective

under the scenarios of a large number of tasks, lacking long-term memory stability in real-world applications.

To address this problem, some methods choose to expand the model during the dynamic learning process in a specific way, leading to interfering with task-specific parameters for each task. For example, a recent work [9] proposed to decompose the model as task-private and task-shared parameters via an additive model parameters decomposition. However, this method only applies an attention vector for the masking of the task-shared parameters. Furthermore, the private parameters were controlled by a regularization and consolidation process, which lead to the linear model increment along with the increasing task number, damaging the *scalability* for deploying a CL system. Another solution to reduce the parameter increase is applying factorization for the model parameters. In this regard, [10] proposed a low-rank factorization method for the model parameters decomposition with a Bayesian process inference. However, this approach required a large rank for achieving desirable accuracy and also suffered from ineffectiveness in some complex data scenarios.

In this work, we propose a low-rank perturbation method to learn the relationship between the learned model (base parameters) and the parameters for new tasks. By formulating a flexible weight transition process, the model parameters during the CL scenario are decomposed as task-shared ones and task-adaptive ones. The former can be adopted from the base task to new tasks. The latter conforms to a low-rank matrix, and the number of relevant parameters can be effectively reduced for every single layer in a neural network across the tasks. With a simple warm-up training strategy, the low-rank task-adaptive parameters can be efficiently initialized with *singular value decomposition*.

Furthermore, to determine which ranks should be pre-

- Corresponding to Fan Zhou (E-mail: fanzhou@buaa.edu.cn).
- Jiaqi Li, Yuanhao Lai, Charles X. Ling, and Boyu Wang are with the Dept. of Computer Science, University of Western Ontario, London, ON, Canada. E-mail: jl3779@uwo.ca. Boyu Wang is also with the Vector Institute, Toronto, ON, Canada.
- Rui Wang, Shichun Yang, and Fan Zhou are with Dept. of Automotive Engineering, Beihang University, Beijing, China.
- Changjian Shui is with Dept. of Electrical and Computer Engineering, McGill University, Montreal, QC, Canada.
- Sabyasachi Sahoo and Christian Gagné are with the Dept. of Electrical Engineering and Computer Engineering, Laval University, Québec City, QC, Canada. Christian Gagné is also with Mila, Québec, Canada.

Manuscript received xxx; revised xxx.

served for the low-rank approximation in different layers in a model, we propose to measure the influences of the introduced low-rank parameters by the *Hessian-aware risk perturbation* across layers of the whole model. This allows the model to automatically assign larger ranks to a layer that contributes more to the final performance under a specific parameter size budget. We theoretically support this approach by providing a formal demonstration that the empirical losses derived from the proposed low-rank perturbation are bounded by the Hessian and the approximation rate of the decomposition. This leads to a Hessian-aware framework that enables the model to determine perturbation ranks that minimize the overall empirical error. Lastly, we apply a pruning technique to control the introduced parameter size and reduce some less important perturbation parameters through the aforementioned Hessian-aware framework by evaluating their importance.

Based on the theoretical analysis, we proposed the **Hessian Aware Low-Rank Perturbation (HALRP)** algorithm, which enables the model to leverage the Hessian information to automatically apply the low-rank perturbation according to a certain approximation rate. To summarize, the contributions of our work mainly lie in three-fold:

- We proposed a Hessian-aware low-rank perturbations framework that allows efficient memory and computation requests for learning continual tasks.
- Theoretical analyses were investigated to show that Hessian information can be used to quantitatively measure the influences of low-rank perturbation on the empirical risk. This leads to an automatic rank selection process to control the model increment.
- Extensive experiments on several benchmarks and recent state-of-the-art baselines (*e.g.*, regularization-, expansion-, and replay-based) were conducted to demonstrate the effectiveness of our method. The results testify the superiority of our HALRP, in terms of accuracy, computational efficiency, scalability, and task-order robustness.

2 RELATED WORK

Regularization-based approaches diminish catastrophic forgetting by penalizing the parameter drift from the previous tasks using different regularizers [4]–[6]. Batch Ensemble [11] designed an ensemble weight generation method by the Hadamard product between a shared weight among all ensemble members and an ensemble member-specific rank-one matrix. [12] indicated that learning tasks in different low-rank vector subspaces orthogonal to each other can minimize task interferences. [13] applied a regularizer with decoupled prototype-based loss, which can improve the intra-class and inter-class structure significantly. Compared to this kind of approach, our method applied task-specific parameters and introduced an explicit weight transition process to leverage the knowledge from the previous tasks and overcome the forgetting issue.

Expansion-based methods utilize different subsets of model parameters for each task. [14] proposed to memorize the learned knowledge by freezing the base model and progressively expanding the new sub-model for new tasks. In [15], the reuse and expansion of networks were achieved

dynamically by selective retraining, with splitting or duplicating components for newly coming tasks. Some work (*e.g.*, [16]) tried to determine the optimal network growth by neural architecture search. To balance memory stability and learning plasticity, [17] adopted a distillation-based method under the class incremental scenario. To achieve the scalability and the robustness of task orders, Additive Parameter Decomposition (APD) [9] adopted sparse task-specific parameters for novel tasks in addition to the dense task-shared ones and performed hierarchical consolidation within similar task groups for the further knowledge sharing. [18] introduced Channel-Wise Linear Reprogramming (CLR) transformations on the output of each convolutional layer of the base model as the task-private parameters. However, this method relied on the prior knowledge from a disjoint dataset (*e.g.*, ImageNet-1K). Winning Subnetworks (WSN) [19] jointly learned the shared network and binary masks for each task. To address the forgetting issue, only the model weights that had not been selected in the previous tasks were tentatively updated during training. But this method still needs to store task-specific masks for the inference stage and relies on extra compression processes for mask encoding to achieve scalability.

Replay-/Memory-based approaches usually leverage different types of replay buffers (*e.g.*, [12], [20]–[25]) to memorize a small episode of the previous tasks, which can be rehearsed when learning the novel ones to avoid forgetting. In [25], a dynamic prototype-guided memory replay module was incorporated with an online meta-learning framework to reduce memory occupation. [26] proposed to process both specific and generalized information by the interplay of three memory networks. To avoid the repeated inferences on previous tasks, Gradient Episodic Memory [2] and its variant [27] projected the new gradients into a feasible region that is determined by the gradients on previous task samples. Instead, Gradient Projection Memory (GPM) [2] chose to directly store the bases of previous gradient spaces to guide the direction of parameters update on new tasks. Compared to these approaches, our proposed method does not rely on extra storage for the data or gradient information of previous tasks, avoiding privacy leakage under some sensitive scenarios.

Low-rank Factorization for CL Low-rank factorization [28] has been widely studied in deep learning to decompose the parameters for model compression [29], [30] or data projection [31], [32]. In the context of CL, [10] considers the low-rank model factorization and automatic rank selection per task for variational inference, which requires significantly large rank increments per task to achieve high accuracy. GPM [2] applied the singular value decomposition on the representations and store them in the memory. [12] proposed to learn tasks by low-rank vector sub-spaces to avoid a joint vector space that may lead to interferences among tasks. The most similar work is Incremental Rank Updates (IRU) [33]. Compared to the decomposition in IRU, we adopted the low-rank approximation on the residual representation in the weights transitions. Furthermore, the rank selection in our work was dynamically and automatically determined according to Hessian-aware perturbations, rather than the manual rank increment in [33].

TABLE 1: List of main notations.

Notation	Description
T, t	Total task number, task index
$\mathcal{T}_t, \mathcal{D}_t$	t -th task, and the related dataset
\mathbf{x}, y	input/sample, class label
\mathbf{W}	model weights
$\mathbf{R}, \mathbf{S}, \mathbf{B}$	task private model weights
$\mathbf{U}, \mathbf{\Sigma}, \mathbf{V}$	SVD decomposition on \mathbf{B} shown in Sect. 3.2
$\text{diag}(\mathbf{\Sigma})$	diagonal elements of $\mathbf{\Sigma}$
$\text{Diag}(\sigma_1, \dots, \sigma_n)$	diagonal matrix with elements $\{\sigma_1, \dots, \sigma_n\}$
$\mathbf{M}^{(k)}$	k -rank low-rank approximation of \mathbf{M}
$\ \cdot\ _F$	Frobenius norm
\mathcal{L}	loss function for the task (e.g, cross-entropy)
\mathcal{L}_{reg}	regularization loss
\mathbf{H}	Hessian matrix
α	loss approximation rate for rank selection
l	layer index in a neural network
\mathbf{g}_l	gradient vector for layer l
r_l	full rank of layer l
k_l	approximated rank for layer l
n	number of total training epochs
n_r	number of warm-up epochs

3 PRELIMINARY AND BACKGROUND

This section introduces the basic knowledge of continual learning and singular value decomposition. In Table 1, we provide a list of the main notations used in our paper. Specifically, the bold uppercase (or lowercase) letters indicate the matrices (or vectors) in the remaining part.

3.1 Continual Learning

Assume the learner receives a series of T tasks $\{\mathcal{T}_0, \dots, \mathcal{T}_{T-1}\}$ sequentially, and denote the dataset of the t^{th} task as $\mathcal{D}_t = \{\mathbf{x}_t^i, y_t^i\}_{i=1}^{N_t}$, where \mathbf{x}_t^i and y_t^i corresponds to the i^{th} instance and label in the total of N_t data points. In the context of CL, the dataset \mathcal{D}_t will become inaccessible after the time step t .

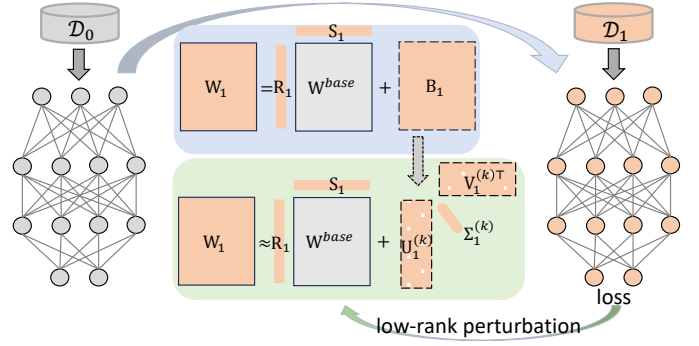
3.2 Low-Rank Approximation of Matrix with SVD

The singular value decomposition (SVD) factorizes a rectangular matrix $\mathbf{B} \in \mathbb{R}^{J \times I}$ with three matrices¹: $\mathbf{B} = \mathbf{U}\mathbf{\Sigma}\mathbf{V}^\top$, where $\mathbf{U} \in \mathbb{R}^{J \times J}$, $\mathbf{V} \in \mathbb{R}^{I \times I}$, and $\mathbf{\Sigma} \in \mathbb{R}^{J \times I}$. Denote the rank of \mathbf{B} with $r \leq \min\{I, J\}$, then \mathbf{B} can be further expressed as $\mathbf{B} = \sum_{i=1}^r \sigma_i \mathbf{u}_i \mathbf{v}_i^\top$, where $\sigma_i \in \text{diag}(\mathbf{\Sigma})$ is the singular values, \mathbf{u}_i and \mathbf{v}_i are respectively the left and right singular vectors. In this work, we take the property of k -rank approximation of \mathbf{B} (with $k \leq r$) by leveraging the *Eckart–Young–Mirsky theorem* [34], which can be expressed with *top- k leading* singular values and vectors: $\mathbf{B}^{(k)} = \mathbf{U}^{(k)} \mathbf{\Sigma}^{(k)} \mathbf{V}^{(k)\top} = \sum_{i=1}^k \sigma_i \mathbf{u}_i \mathbf{v}_i^\top$, where $\mathbf{U}^{(k)}$, $\mathbf{\Sigma}^{(k)}$, $\mathbf{V}^{(k)}$ are the corresponding *leading principal sub-matrices*². k is chosen to tolerate a certain approximation error under the Frobenius norm $\|\cdot\|_F$ (See Appendix A for the proof):

$$\|\mathbf{B} - \mathbf{B}^{(k)}\|_F = \sqrt{\sigma_{k+1}^2 + \dots + \sigma_r^2} \quad (1)$$

1. In this paper, we assume the eigenvalues are always sorted with descending order in such SVD decompositions, i.e., $\sigma_1 \geq \sigma_2 \geq \dots \geq \sigma_r$.

2. With a slight abuse of notation, the notation $\mathbf{M}^{(k)}$ refers to the k -rank approximation of the matrix \mathbf{M} according to the context: (1) $\mathbf{U}^{(k)}$, $\mathbf{\Sigma}^{(k)}$, $\mathbf{V}^{(k)}$ indicate the top- k leading submatrices; (2) $\mathbf{B}^{(k)}$ means the r -rank low-rank approximation for \mathbf{B} , then same for $\mathbf{W}^{(k)}$.

Fig. 1: Low rank decomposition between \mathcal{T}_1 and \mathcal{T}_0

4 METHODOLOGY

Our framework leverages the low-rank approximation of neural network weights. In the following parts, we present the methodology for handling the fully connected layers and the convolutional layers. The analysis herein can be applied to any layer of the model. Without loss of generality, we omit the layer index l in this section. For simplicity, we illustrate the learning process using tasks \mathcal{T}_0 and \mathcal{T}_1 in Sections 4.1 and 4.2, which can be applied to the successive new tasks as shown in Section 4.5.

4.1 Fully Connected Layers

We first consider linear layers of neural networks. We begin by learning task \mathcal{T}_0 without any constraints on the model parameters. Specifically, we train the model by minimizing the empirical risk to get the base weights $\mathbf{W}^{\text{base}} = \arg \min_{\mathbf{W}} \mathcal{L}(\mathbf{W}; \mathcal{D}_0)$, where $\mathbf{W}^{\text{base}} \in \mathbb{R}^{J \times I}$, J is the output dimension, and I is the input dimension of the layer.

Then, when the task \mathcal{T}_1 comes to the learner, we can train the model fully on \mathcal{D}_1 and get the updated weights $\mathbf{W}_1 \in \mathbb{R}^{J \times I}$. However, undesired model drifts can lead to worse performance on \mathcal{T}_0 if no constraints are applied to the parameters update. Previous work [4] applied a L_2 regularization to enforce that the weights learned on the new model will not be too far from those of the previous tasks. Although this kind of method only expands the base model with limited parameters, it can lead to worse performance on both \mathcal{T}_0 and \mathcal{T}_1 .

To pursue a better trade-off between the model size increment and overall performance on both \mathcal{T}_0 and \mathcal{T}_1 , we assume the unconstrained trained parameters \mathbf{W}_1 on \mathcal{T}_1 can be transformed from \mathbf{W}^{base} by the *low-rank weight perturbation* (LRWP, as illustrated in Figure 1),

$$\mathbf{W}_1 = \mathbf{R}_1 \mathbf{W}^{\text{base}} \mathbf{S}_1 + \mathbf{B}_1 \quad (2)$$

where $\mathbf{B}_1 \in \mathbb{R}^{J \times I}$ is a sparse low-rank matrix, $\mathbf{R}_1 = \text{Diag}(r_{1,0}, \dots, r_{1,J})$, and $\mathbf{S}_1 = \text{Diag}(s_{1,0}, \dots, s_{1,I})$ are task-private parameters for \mathcal{T}_1 ³.

The form of the proposed low-rank decomposition in Eq. 2 has differences with the additive parameter decomposition proposed in [9]. In fact, the task-adaptive bias term

3. We will show later that \mathbf{B} can be further approximated by $\mathbf{U}^{(k)}$, $\mathbf{\Sigma}^{(k)}$, $\mathbf{V}^{(k)}$ with low-rank approximation, so we can write the task-private weights for task t as either $\{\mathbf{R}_t, \mathbf{S}_t, \mathbf{B}_t^{(k)}\}$ or $\{\mathbf{R}_t, \mathbf{S}_t, \mathbf{U}_t^{(k)}, \mathbf{\Sigma}_t^{(k)}, \mathbf{V}_t^{(k)}\}$.

\mathbf{B}_1 conforms to a low-rank matrix, which reduces both the parameter storage and the computational overhead. Moreover, the task-adaptive mask terms \mathbf{R}_1 and \mathbf{S}_1 include both row-wise and column-wise scaling parameters instead of only column-wise parameters like [9] to allow smaller and possibly sparser discrepancy: $\mathbf{B}_1 = \mathbf{W}_1 - \mathbf{R}_1 \mathbf{W}^{\text{base}} \mathbf{S}_1$.

In addition, regarding the parameter estimation, we can substitute \mathbf{B}_1 with its k -rank decomposition $\mathbf{B}_1^{(k)} = \sum_{i=1}^k \sigma_i \mathbf{u}_i \mathbf{v}_i^\top$ in Eq. 2 and directly minimize the empirical risk on task \mathcal{T}_1 to get the parameter estimation through stochastic gradient descent with the random initialization of $\{\mathbf{u}_i\}_{i=1}^k$ and $\{\mathbf{v}_i\}_{i=1}^k$. However, in practice, we found it challenging to learn a useful decomposition in this way (*i.e.*, the estimations converge to a local optimum quickly) and the empirical risk minimization does not benefit from the low-rank decomposition. Due to the homogeneity among the one-rank components $\{\mathbf{u}_i \mathbf{v}_i^\top\}_{i=1}^k$, random initialization cannot sufficiently distinguish them and hence make the gradient descent ineffective.

To address the aforementioned ineffective training problem, we first train the model fully on task \mathcal{T}_1 for a few epochs (*e.g.*, one or two) to get rough parameter estimations $\mathbf{W}_1^{\text{free}} \in \mathbb{R}^{J \times I}$ of the new task, indicating free-trained weights without any constraints. Then, a good warm-up initialized values for Eq. 2 can then be obtained by solving the following least squared error (LSE) minimization objective,

$$\arg \min_{\mathbf{R}, \mathbf{S}, \mathbf{B}} \|\mathbf{W}_1^{\text{free}} - \mathbf{R} \mathbf{W}^{\text{base}} \mathbf{S} - \mathbf{B}\|_F^2 \quad (3)$$

As $\mathbf{R}, \mathbf{S}, \mathbf{B}$ can correlate, minimizing them simultaneously can be difficult. Thus, we minimize Eq. 3 alternately. First, fix \mathbf{S}, \mathbf{B} and solve \mathbf{R} , and so on.

$$\begin{aligned} \mathbf{R}_1^{\text{free}} &= \arg \min_{\mathbf{R}} \|\mathbf{W}_1^{\text{free}} - \mathbf{R} \mathbf{W}^{\text{base}}\|_F^2 \\ \mathbf{S}_1^{\text{free}} &= \arg \min_{\mathbf{S}} \|\mathbf{W}_1^{\text{free}} - \mathbf{R}_1^{\text{free}} \mathbf{W}^{\text{base}} \mathbf{S}\|_F^2 \\ \mathbf{B}_1^{\text{free}} &= \mathbf{W}_1^{\text{free}} - \mathbf{R}_1^{\text{free}} \mathbf{W}^{\text{base}} \mathbf{S}_1^{\text{free}} \end{aligned} \quad (4)$$

Eq. 4 can be solved efficiently via LSE minimization. For example, for \mathbf{R} , we have $\|\mathbf{W}_1^{\text{free}} - \mathbf{R} \mathbf{W}^{\text{base}}\|_F^2 = \sum_{i=1}^I \sum_{j=1}^J (w_{ji}^{\text{free}} - r_j w_{ji}^{\text{base}})^2$, where w_{ji}^{free} and w_{ji}^{base} are the elements of j -th row and i -th column of $\mathbf{W}_1^{\text{free}}$ and \mathbf{W}^{base} , respectively. Applying the derivative *w.r.t.* r_j and let it equals 0, we have $r_j = \sum_i w_{ji}^{\text{free}} w_{ji}^{\text{base}} / \sum_i (w_{ji}^{\text{base}})^2$. Then, we can solve \mathbf{S} and \mathbf{B} (see Appendix C for more details). Furthermore, with the SVD solver denoted by $\text{SVD}(\cdot)$, the values of the low-rank decomposition for $\mathbf{B}_1^{\text{free}}$ can be obtained:

$$\mathbf{U}_1^{\text{free}}, \mathbf{\Sigma}_1^{\text{free}}, \mathbf{V}_1^{\text{free}} = \text{SVD}(\mathbf{B}_1^{\text{free}}) \quad (5)$$

A k -rank approximation $\mathbf{U}_1^{(k)\text{free}}, \mathbf{\Sigma}_1^{(k)\text{free}}, \mathbf{V}_1^{(k)\text{free}}$ can be obtained by retaining their corresponding leading principal submatrix of order $k \leq r$. So we can obtain a k -rank approximation⁴ to $\mathbf{W}_1^{\text{free}}$ by

$$\mathbf{W}_1^{\text{free}} \approx \mathbf{W}_1^{(k)\text{free}} = \mathbf{R}_1^{\text{free}} \mathbf{W}^{\text{base}} \mathbf{S}_1^{\text{free}} + \mathbf{B}_1^{(k)\text{free}}, \quad (6)$$

where $\mathbf{B}_1^{(k)\text{free}} = \mathbf{U}_1^{(k)\text{free}} \mathbf{\Sigma}_1^{(k)\text{free}} (\mathbf{V}_1^{(k)\text{free}})^\top$.

4. With this approximation, the extra parameters introduced for each successive task will be $\mathcal{O}((I+J)(k+1)+k)$. Then the model increment ratio is $\rho = \frac{\text{size}\{\mathbf{R}, \mathbf{S}, \mathbf{U}^{(k)}, \mathbf{\Sigma}^{(k)}, \mathbf{V}^{(k)}\}}{\text{size}\{\mathbf{W}^{\text{base}}\}} = \frac{(I+J)(k+1)+k}{IJ} \ll 1$ in practice.

Finally, we can initialize the values in Eq. 2 with $\mathbf{R}_1^{\text{free}}, \mathbf{S}_1^{\text{free}}, \mathbf{U}_1^{(k)\text{free}}, \mathbf{\Sigma}_1^{(k)\text{free}}$ and $\mathbf{V}_1^{(k)\text{free}}$, and then fine-tune their estimates by minimizing the empirical risk on task \mathcal{T}_1 to achieve better performance. The proposed training technique not only enables well-behaved estimations of the low-rank components but also sheds light on how to select approximation ranks of different layers to achieve an optimal trade-off between model performance and parameter size, as discussed in Section 4.3.

4.2 Convolutional Layers

In addition, we can decompose the weights of a convolutional layer in a similar way. Suppose that the size of the convolutional kernel is $d \times d$. The base weights of the convolution layer for task \mathcal{T}_0 would be a tensor $\mathbf{W}_{\text{conv}}^{\text{base}} \in \mathbb{R}^{d \times d \times J \times I}$. Similar to Eq. 2, a low-rank weight perturbation for transforming $\mathbf{W}_{\text{conv}}^{\text{base}}$ to $\mathbf{W}_{\text{conv},1} \in \mathbb{R}^{d \times d \times J \times I}$ is,

$$\mathbf{W}_{\text{conv},1} = \mathbf{R}_{\text{conv},1} \otimes \mathbf{W}_{\text{conv}}^{\text{base}} \otimes \mathbf{S}_{\text{conv},1} \oplus \mathbf{B}_{\text{conv},1} \quad (7)$$

where $\mathbf{R}_{\text{conv},1} \in \mathbb{R}^{1 \times 1 \times J \times 1}$, $\mathbf{S}_{\text{conv},1} \in \mathbb{R}^{1 \times 1 \times 1 \times I}$ and $\mathbf{B}_{\text{conv},1} \in \mathbb{R}^{1 \times 1 \times J \times I}$ is sparse low-rank tensor (matrix), \otimes and \oplus are element-wise tensor multiplication and summation operators will automatically expand tensors to be of equal sizes, following the broadcasting semantics of some popular scientific computation package like Numpy [35] or PyTorch [36]. Thus, the number of parameters added through this kind of decomposition is still $\mathcal{O}(I+J)$.

To get the estimations of the introduced parameters, we can solve a similar LSE problem as in Eq. 3 to obtain initial estimates $\mathbf{R}_{\text{conv},1}^{\text{free}}$ and $\mathbf{S}_{\text{conv},1}^{\text{free}}$. Then we take the average of the first two dimensions to transform the discrepancy tensor $(\mathbf{W}_{\text{conv},1}^{\text{free}} - \mathbf{R}_{\text{conv},1}^{\text{free}} \otimes \mathbf{W}_{\text{conv}}^{\text{base}} \otimes \mathbf{S}_{\text{conv},1}^{\text{free}})$ to be a $1 \times 1 \times J \times I$ tensor, which can then be applied a similar decomposition with the linear layers (Eq. 5 and 6.) to obtain the low-rank estimates of $\mathbf{B}_{\text{conv},1}^{\text{free}}$.

4.3 Rank Selection for each layer based on Hessian Information

Sections 4.1 and 4.2 present how the low-rank approximation can be used to transfer knowledge and reduce the number of parameters for a single layer across the tasks in continual learning. However, how to select the preserved rank for each layer remains unsolved. We tackle this problem by measuring how the empirical risk $\mathcal{L}(\mathbf{W})$ is influenced by the introduced low-rank parameters across different layers so that we can assign a larger rank to a layer that contributes more to the risk. Inspired by the previous studies [37], [38] about the relationship between Hessian and quantization errors, we establish the following Theorem 1. The full proof is presented in Appendix B.

Theorem 1. *Assume that a neural network of L layers with vectorized weights $(\omega_1^*, \dots, \omega_L^*)$ that have converged to local optima, such that the first and second order optimality conditions are satisfied, *i.e.*, the gradient is zero, and the Hessian is positive semi-definite. Suppose a perturbation $\Delta \omega_1^*$ applied to the first layer weights, then we have the loss increment*

$$\begin{aligned} \mathcal{L}(\omega_1^* - \Delta \omega_1^*, \dots, \omega_L^*) - \mathcal{L}(\omega_1^*, \dots, \omega_L^*) \\ \leq \frac{1}{2} \mathbf{H}_1 \|\Delta \omega_1^*\|_F^2 + o(\|\Delta \omega_1^*\|_F^2), \end{aligned} \quad (8)$$

where $\mathbf{H}_1 = \Delta \mathcal{L}(\omega_1^*)$ is the Hessian matrix at only the variables of the first layer weights.

Remark: Theorem 1 demonstrated the relationship between the perturbation Δw_1^* on weights and the effect on the loss objective $\Delta \mathcal{L}$. Specifically, when a weight perturbation Δw_1^* is applied to the related weight matrix w_1^* , the perturbation introduced on the loss function is upper bounded mainly by the product of the Frobenius norms of Hessian matrix (i.e., $\|\mathbf{H}_1\|_F$) and weight perturbation (i.e., $\|\Delta w_1^*\|_F^2$). It further inspires us to follow this rule to select the proper ranks by considering the low-rank approximation in the previous section as a perturbation to the model weights.

In our low-rank perturbation setting, we assume that $\mathbf{W}_1^{\text{free}}$ by warm-up training is a local optimum. By Theorem 1, we consider the difference between $\mathbf{W}_1^{\text{free}}$ and its k -rank approximation $\mathbf{W}_1^{(k)\text{free}}$ as a perturbation $\Delta \mathbf{W}_1^{(k)\text{free}}$ for the weights. Then the amount of perturbation can be computed with the low-rank approximation error:

$$\|\Delta \mathbf{W}_1^{(k)\text{free}}\|_F = \|\mathbf{W}_1^{\text{free}} - \mathbf{W}_1^{(k)\text{free}}\|_F = \sqrt{\sum_{i=k+1}^r \sigma_i^2} \quad (9)$$

where $\{\sigma_i\}_{i=1}^r$ are the singular values of $\mathbf{W}_1^{\text{free}}$ and r is the matrix rank of $\mathbf{W}_1^{\text{free}}$.

Thus, according to Theorem 1, the influence on the loss introduced by this low-rank weight perturbation is given by

$$\begin{aligned} & \mathcal{L}(\mathbf{W}_1^{\text{free}} - \Delta \mathbf{W}_1^{(k)\text{free}}) - \mathcal{L}(\mathbf{W}_1^{\text{free}}) \\ & \leq \frac{1}{2} \mathbf{H}_1 \|_F \left(\sum_{i=1}^k \sigma_i^2 \right) + o\left(\sum_{i=k+1}^r \sigma_i^2 \right). \end{aligned} \quad (10)$$

where the Hessian matrix \mathbf{H}_1 can be approximated by the negative empirical Fisher information [39], i.e., the outer product of the gradient vector for the layer weights. So $\|\mathbf{H}_1\|_F$ can be approximated by $\|\mathbf{g}_1\|_2^2$, where $\mathbf{g}_1 = \frac{\partial \mathcal{L}}{\partial \mathbf{W}_1} |_{\mathbf{W}_1 = \mathbf{W}_1^{\text{free}}}$. Finally, we can quantitatively measure the contribution of the loss of adding a marginal rank k for a particular layer l by $\|\mathbf{g}_l\|_2^2 \sigma_{l,k}^2$, where \mathbf{g}_l is the gradient for the layer- l weights and $\sigma_{l,k}$ is the k -th singular value of the free-trained layer- l weights, and sort them by the descending order of importance.

For a given loss approximation rate α (e.g., 0.9), we can determine the rank k_l (with $k_l \leq r_l$ where r_l is the total rank of the layer l) for each layer $l = 0, \dots, L-1$ by solving

$$\begin{aligned} & \min_{k_1, \dots, k_{L-1}} \sum_{l=0}^{L-1} \sum_{i=1}^{k_l} \|\mathbf{g}_l\|_2^2 \sigma_{l,i}^2 \\ & \text{s.t. } \sum_{l=0}^{L-1} \sum_{i=1}^{k_l} \|\mathbf{g}_l\|_2^2 \sigma_{l,i}^2 \geq \alpha \sum_{l=0}^{L-1} \sum_{i=1}^{r_l} \|\mathbf{g}_l\|_2^2 \sigma_{l,i}^2 \end{aligned} \quad (11)$$

Remark: Eq. 11 enables a dynamic scheme for the trade-off between the approximation precision and computational efficiency. For a given approximation rate, the model can automatically select the rank for all the layers in the model.

4.4 Regularization and Pruning on Parameters

The proposed low-rank perturbation method introduced extra parameters compared to a single-task model. For these

Algorithm 1 Hessian Aware Low-Rank Perturbation

Require: Task data $\{\mathcal{D}_t\}_{t=1}^T$; total epochs for one task n ; rank estimation epochs n_r ; parameter increments limitation ratio p , approximation rate α .

Ensure: Base weights \mathbf{W}^{base} and $\{\mathbf{W}_t^*\}_{t=1}^{T-1}$ for each task.

- 1: Obtain $\mathbf{W}^{\text{base}} = \arg \min_{\mathbf{W}} \mathcal{L}(\mathbf{W}; \mathcal{D}_0)$ on task \mathcal{T}_0 .
- 2: **for** $t = 1, \dots, T-1$ **do**
- 3: Warm-up pre-training on task \mathcal{T}_t for n_r epochs: $\mathbf{W}_t^{\text{free}} = \arg \min_{\mathbf{W}} L(\mathbf{W}; \mathcal{D}_t)$.
- 4: Low-rank decomposition for all layers via Eq. 2 or Eq. 7: $\mathbf{W}_t^{\text{free}} = \mathbf{R}_t^{\text{free}} \mathbf{W}_t^{\text{base}} \mathbf{S}_t^{\text{free}} + \mathbf{B}_t^{\text{free}}$.
- 5: Apply $\mathbf{U}_t^{(k)\text{free}}, \mathbf{\Sigma}_t^{(k)\text{free}}, \mathbf{V}_t^{(k)\text{free}} = \text{SVD}(\mathbf{B}_t^{\text{free}})$.
- 6: Select the ranks k_l for each layer l through Eq. 11.
- 7: Re-initialize the task \mathcal{T}_t parameters with Eq. 6.
- 8: Fine-tuning on \mathcal{T}_t for $(n - n_r)$ epochs with:

$$\mathbf{W}_t^* = \arg \min_{\mathbf{W}} \mathcal{L}(\mathbf{W}; \mathcal{D}_t) + \mathcal{L}_{\text{reg}}(\mathbf{W}) \quad (13)$$

- 9: If the size of the introduced parameters is larger than a threshold p , apply the pruning method in Section 4.4.
- 10: **end for**
- 11: **return** \mathbf{W}^{base} and $\{\mathbf{W}_t^*\}_{t=1}^{T-1}$.

parameters, we can further add regularization to avoid overfitting. To control the model growth, we can further prune the introduced parameters to improve memory efficiency.

Firstly, by following [9], we can add regularizations on $\mathbf{U}^{(k)\text{free}}, \mathbf{V}^{(k)\text{free}}, \mathbf{R}^{\text{free}}, \mathbf{S}^{\text{free}}$ since second task \mathcal{T}_1 to enhance the sparsity of the task-private parameters (see Appendix D for more discussion for this fine-tuning objective):

$$\begin{aligned} \mathcal{L}_{\text{reg}}(\mathbf{W}_t) = & \sum_l \left[\lambda_0 (\|\mathbf{U}_{t,l}^{(k_l)\text{free}}\| + \|\mathbf{V}_{t,l}^{(k_l)\text{free}}\|) \right. \\ & + \lambda_1 (\|\mathbf{R}_{t,l}^{\text{free}}\|_2^2 + \|\mathbf{S}_{t,l}^{\text{free}}\|_2^2) \\ & \left. + \|\mathbf{U}_{t,l}^{(k_l)\text{free}}\|_2^2 + \|\mathbf{V}_{t,l}^{(k_l)\text{free}}\|_2^2 \right] \end{aligned} \quad (12)$$

where λ_0, λ_1 are balancing coefficients, and the subscripts (t, l) indicate the relevant weights for layer l in task t .

Secondly, we can also prune the extra parameters by setting zero values for elements whose absolute values are lower than a certain threshold. The threshold can be selected in the following three ways:

- (1) Pruning via absolute value: a fixed tiny positive value (e.g., 10^{-5}) is set for the threshold.
- (2) Pruning via relative percentile: to control the ratio of increased parameter size over a single-task model size under γ , the pruning threshold is selected as the $(1 - \gamma)$ -percentile of the low-rank parameters among all layers of all tasks.
- (3) Pruning via mixing absolute value and relative percentile: we set a threshold as the maximum of the thresholds obtained from the above two methods to prune using relative percentiles.

4.5 Summary of Algorithm

In the previous sections, we described the model update from \mathcal{T}_0 to \mathcal{T}_1 with an illustrative example. The overall description of our proposed HALRP is shown in Algorithm 1.

At the start, the learner was trivially trained on the first task \mathcal{T}_0 to obtain \mathbf{W}^{base} . As for each incoming task \mathcal{T}_t with $t = 1, \dots, T - 1$, we first train the model without any constraints for n_r epochs to get a rough initialization $\mathbf{W}_t^{\text{free}}$. Secondly, we apply the low-rank decomposition on all layers with Eq. 2 (for linear layers) for Eq. 7 (for convolutional layers) by solving a least square error minimization problem described in Eq. 4. Then, we further apply the singular value decomposition for the residual matrix $\mathbf{B}_t^{\text{free}}$. With this decomposition, we can measure the Hessian-aware perturbations and the rank k_l for each layer l through Eq. 11. After the rank selection, we can re-initialize the model parameters with the approximated weights $\mathbf{W}_t^{(k)\text{free}} \approx \mathbf{W}_t^{\text{free}}$ and then fine-tune the model for the remaining $n - n_r$ epochs to obtain the optimal weights for \mathcal{T}_t . As for the inference stage, the base weights and the task-specific parameters can be adopted to make predictions for each task.

5 EXPERIMENTAL RESULTS

We first compare the accuracy over several recent baselines with standard CL protocol. Then, we studied the task order robustness, forgetting, memory cost, training time efficiency, and the ablation study to show the effectiveness further. We briefly describe the experimental setting herein while delegating more details in Appendix F.

5.1 Experimental Settings

Datasets: We evaluate the algorithm on the following datasets: 1) **CIFAR100-Split:** Split the classes into 10 groups; for each group, consider a 10-way classification task. 2) **CIFAR100-SuperClass:** It consists of images from 20 superclasses of the CIFAR-100 dataset. 3) **Permuted MNIST (P-MNIST):** obtained from the MNIST dataset by random permutations of the original MNIST pixels. We follow [40] to create 10 sequential tasks using different permutations, and each task has 10 classes. 4) **Five-dataset:** It uses a sequence of 5 different benchmarks including CIFAR10 [41], MNIST [42], notMNIST [43], FashionMNIST [44] and SVHN [45]. Each benchmark contains 10 classes. 5) **Omniglot Rotation** [46]: 100 12-way classification tasks. The rotated images in 90° , 180° , and 270° are generated by following [9]. 6) **TinyImageNet:** a variant of ImageNet [47] dataset containing 200 classes. Here, we adopted two settings, one with 20 10-way classification tasks (**TinyImageNet 20-split**) and another more challenging setting with 40 5-way classification tasks (**TinyImageNet 40-split**).

Baselines: We compared the following baselines by the publicly released code or our re-implementation: **STL:** single-task learning with individual models for each task. **MTL:** multi-task learning with a single for all the tasks simultaneously [48]. **EWC:** *Elastic Weight Consolidation* method proposed by [4]. **L2:** the model is trained with L_2 -regularizer [4] $\lambda \|\boldsymbol{\theta}_t - \boldsymbol{\theta}_{t-1}\|_2^2$ between the current model and the previous one. **BN:** The *Batch Normalization* method [49]. **BE:** The *Batch Ensemble* method proposed by [11]. **APD:** The *Additive Parameter Decomposition* method [9]. Each layer of the target network was decomposed into task-shared and task-specific parameters with mask vectors. **APDfix:** We modify the APD method by fixing the model parameters

while only learning the mask vector when a new task comes to the learner. **IBPWF:** Determine the model expansion with non-parametric Bayes and weights factorization [10]. **GPM** [2]: A replay-based method by orthogonal gradient descent. **WSN** [19]: Introduce learnable weight scores to generate task-specific binary masks for optimal subnetwork selection. **BMKP** [50]: A bilevel memory framework for knowledge projection: a working memory to ensure plasticity and a long-term memory to guarantee stability. **CLR** [18]: An *expansion-based* method by applying Channel-Wise Linear Reprogramming transformations on each convolutional layer in the base model. This method originally relies on a model pre-trained on an extra dataset (i.e., ImageNet-1K) disjoint with the above task datasets, rather than the *train-from-scratch* manner adopted by other baselines. To make a fair comparison, we pre-trained the base model on the first task of the above task datasets and applied it to all tasks. **PRD** [51]: Prototype-sample relation distillation with supervised contrastive learning. Furthermore, we also compared our methods with **IRU** [33], a method also based on the low-rank decomposition. However, due to the code limitation⁵ of **IRU** [33], we further implemented our method under the dataset protocol and model architecture setting in [33] and compared our performance with the results reported in [33]. For the implementation of all the methods, we applied the same hyperparameters (e.g., batch size, training epochs, regularization coefficient) to realize fair comparisons. See Appendix F.3 for more details.

Model Architecture: For CIFAR100-Split, CIFAR100-SuperClass, and P-MNIST datasets, we adopted LeNet as the base model. As for Five-dataset and ImageNet datasets, we evaluated with AlexNet and reduced ResNet18 networks where the latter has reduced filters compared to standard ResNet18 (see Appendix F.2). And we followed [19] to use an extended LeNet model on the Omniglot-Rotation dataset.

Evaluation Metrics: We mainly adopted the average of the accuracies of the final model on all tasks (we simply call “accuracy” or “Acc.” later) for the empirical comparisons. As for the forgetting statistics, we applied backward transfer (BWT) [2] as a quantitative measure. Especially, we also compared the order-robustness of different methods by calculating the *Order-normalized Performance Disparity* that will be introduced later. For each single experiment (e.g., each task order), we repeat with five random seeds to compute the average and standard error.

5.2 Empirical Accuracy

We provide the average accuracies on the six benchmarks in Table 2 and Table 3. From these numerical results, we can conclude our method achieved state-of-the-art performances compared to the baseline methods. From these numerical results, we can conclude our method achieved state-of-the-art performances compared to the baseline methods.

According to the evaluations on CIFAR100-Split and CIFAR100-SuperClass in Table 2, we can observe that our proposed HALRP outperforms the recent methods (e.g., GPM (replay-based), APD and WSN (expansion-based)) with a significant margin (e.g., with an improvement about

⁵ IRU code only contains the implementation on the multi-layer perceptron. See <https://github.com/CSIPlab/task-increment-rank-update>

Method	CIFAR100-Split (with LeNet)				CIFAR100-SuperClass (with LeNet)			
	5%	25%	50%	100%	5%	25%	50%	100%
STL	45.13 ± 0.04	59.04 ± 0.03	64.38 ± 0.06	69.55 ± 0.06	43.76 ± 0.68	56.09 ± 0.07	60.06 ± 0.06	64.47 ± 0.05
MTL	44.95 ± 0.11	60.21 ± 0.28	65.65 ± 0.20	69.70 ± 0.28	40.43 ± 0.15	49.88 ± 0.27	53.83 ± 0.27	55.62 ± 0.41
L2	37.15 ± 0.21	48.86 ± 0.28	53.35 ± 0.34	58.09 ± 0.43	34.03 ± 0.08	43.40 ± 0.27	46.10 ± 0.28	48.75 ± 0.24
EWC	37.76 ± 0.20	50.09 ± 0.38	55.65 ± 0.40	60.53 ± 0.26	33.70 ± 0.32	44.02 ± 0.39	47.35 ± 0.47	49.97 ± 0.39
BN	37.60 ± 0.17	50.70 ± 0.28	54.79 ± 0.28	60.34 ± 0.40	36.76 ± 0.14	48.20 ± 0.16	51.43 ± 0.16	55.44 ± 0.19
BE	37.63 ± 0.15	51.13 ± 0.3	55.37 ± 0.28	61.09 ± 0.33	37.05 ± 0.20	48.48 ± 0.14	51.78 ± 0.17	55.97 ± 0.17
APD	36.60 ± 0.14	54.59 ± 0.07	59.71 ± 0.03	66.54 ± 0.03	32.81 ± 0.29	49.00 ± 0.06	52.64 ± 0.19	60.54 ± 0.23
APDfix	35.66 ± 0.33	54.62 ± 0.11	59.86 ± 0.24	66.64 ± 0.14	24.27 ± 0.22	48.71 ± 0.11	53.42 ± 0.12	61.47 ± 0.16
IBWPF	38.35 ± 0.26	47.87 ± 0.25	53.46 ± 0.13	57.13 ± 0.15	33.09 ± 0.50	51.32 ± 0.27	52.52 ± 0.26	55.98 ± 0.33
GPM	32.86 ± 0.35	51.61 ± 0.22	57.60 ± 0.19	64.49 ± 0.10	34.88 ± 0.30	47.31 ± 0.51	51.23 ± 0.55	57.91 ± 0.28
WSN	37.01 ± 0.63	55.21 ± 0.59	61.56 ± 0.42	66.56 ± 0.49	36.89 ± 0.49	52.42 ± 0.62	58.23 ± 0.38	61.81 ± 0.54
BMKP	42.36 ± 0.90	56.81 ± 1.05	62.87 ± 0.60	66.95 ± 0.53	37.26 ± 0.87	53.62 ± 0.59	57.76 ± 0.66	61.97 ± 0.19
CLR	36.46 ± 0.29	51.44 ± 0.35	57.00 ± 0.43	61.83 ± 0.60	37.93 ± 0.25	49.82 ± 0.56	53.86 ± 0.63	57.07 ± 0.60
PRD	31.58 ± 0.29	56.07 ± 0.22	59.61 ± 0.33	62.74 ± 0.45	33.34 ± 0.48	52.99 ± 0.28	55.85 ± 0.45	57.80 ± 0.50
HALRP	45.09 ± 0.05	58.94 ± 0.09	63.61 ± 0.08	67.92 ± 0.17	43.84 ± 0.04	54.93 ± 0.04	58.68 ± 0.11	62.56 ± 0.30

TABLE 2: Accuracies \uparrow on CIFAR100-Split/-SuperClass with different percentages of training data.

1% ~ 3%). Especially, we also evaluated the performances of all the methods under different amounts of training data (*i.e.*, 5% ~ 100%) on these two benchmarks. It was interesting to see that our proposed method had advantages in dealing with extreme cases with limited data. Compared to other methods, the performance margins become more significant with fewer training data. For example, on CIFAR100-Split, our proposed HALRP outperforms APD and WSN with an improvement of 1.28% and 1.36% respectively, but these margins will dramatically rise to ~ 8% if we reduce the training set to 5% of the total data. These results showed that our method can work better under these extreme cases.

On Five-dataset, we adopted two kinds of neural networks, *i.e.*, AlexNet and ResNet18, to verify the effectiveness of HALRP under different backbones. We can observe that our method consistently outperforms the other methods under different backbones, indicating the applicability and flexibility for different model choices. Compared with the analyses in the following part, we can conclude that our method is also robust under different orders of the tasks.

Especially, we also conducted experiments on the Omniglot-Rotation dataset to demonstrate the scalability of our method. We follow [19] to learn the 100 tasks under the default sequential order. The average accuracy was shown in Table 3c. We demonstrate that our method is applicable to a large number of tasks and can still achieve comparable performance with limited model increment.

On TinyImageNet dataset, we evaluated our methods on two settings, one with 20-split and another with 40-split, and the results are posted in Table 3d. According to the empirical results, we can conclude that our proposed method can perform well on this challenging dataset, with a better trade-off between the average accuracy and task order robustness. Compared to the previous methods APD and APDfix that aim to address the issue of task order robustness, our HALRP can perform well in a more consistent manner. Furthermore, our methods also have advantages regarding computational efficiency and memory consumption that we will discuss later in the following sections.

Additionally, we also provide comparisons with IRU [33] that is also based on low-rank decomposition. We note that the official code of IRU only contains a demo for multi-layer perceptron (MLP), and no complete code for the

convolutional network (even LeNet) can be found. Due to this limitation, we cannot implement IRU under our setting. To make fair comparisons, we re-implement our method under the setting of IRU [33]. We describe the setting as follows: 1) Dataset Protocol: [33] generated 20 random tasks on PMNIST, rather than 10 tasks in this work. Moreover, [33] randomly divided the CIFAR100 dataset into 20 tasks, rather than the superclass-based splitting in our paper. Thus, we denote the two datasets in [33] as “PMNIST-20” and “CIFAR100-20”, to distinguish them from the “PMNIST” and “CIFAR100-SuperClass” used in the common setting. (2) Model Architecture: Apart from the architectures we introduced before, we also follow the MLP used in [33], a three-layer (fully-connected) multilayer perceptron with 256 hidden nodes. The results of our method and IRU are listed in Table 4. We can conclude that our method achieved a large performance gain compared to IRU.

In the following parts, we will further investigate the empirical performance under different aspects, *i.e.*, task order robustness, forgetting statistics, model growth, and time complexity. We will show that our proposed method can achieve a better trade-off among these realistic metrics apart from the average accuracy.

5.3 Robustness on Task Orders

We evaluate the robustness of these algorithms under different task orders. Following the protocol of [9], we assessed the task order robustness with the **Order-normalized Performance Disparity** (OPD) metric, which is computed as the disparity between the performance \bar{P}_t^R of task t on R random task sequences: $OPD_t \triangleq \max\{\bar{P}_t^1, \dots, \bar{P}_t^R\} - \min\{\bar{P}_t^1, \dots, \bar{P}_t^R\}$. The maximum OPD (MOPD) and average OPD (AOPD) are defined by

$$\begin{aligned} MOPD &\triangleq \max\{OPD_1, \dots, OPD_T\} \\ AOPD &\triangleq \frac{1}{T} \sum_{t=1}^T OPD_t \end{aligned} \quad (14)$$

respectively.

Thus, smaller AOPD and MOPD indicate better task-order robustness. For CIFAR100-Split and SuperClass datasets, we adopted different orders by following [9]. For the P-MNIST and Five-dataset, we report the averaged

P-MNIST LeNet				Five-dataset						Omniglot-Rotation LeNet				
Method				Method	AlexNet			ResNet-18			Method			
	Acc.↑	MOPD↓	AOPD↓		Acc.↑	MOPD↓	AOPD↓	Acc.↑	MOPD↓	AOPD↓		Acc.↑	MOPD↓	AOPD↓
STL	98.24±0.01	0.15	0.09	STL	89.32±0.06	0.74	0.30	94.24±0.05	0.67	0.24	STL	80.93±0.18	20.83	3.42
MTL	96.70±0.07	1.58	0.81	MTL	88.02±0.18	2.08	0.68	93.82±0.06	0.67	0.30	MTL	93.95±0.11	6.25	2.11
L2	79.14±0.70	29.66	18.94	L2	78.24±2.00	35.11	15.35	85.94±2.79	37.03	12.72	L2	69.86±1.23	17.23	6.96
EWC	81.69±0.86	21.51	12.16	EWC	78.44±2.20	33.29	13.18	86.32±2.80	33.84	11.80	EWC	69.75±1.28	21.39	7.02
BN	81.04±0.15	19.77	8.18	BN	82.35±2.45	34.83	12.56	88.36±2.21	30.22	9.55	BN	77.08±0.86	14.41	5.58
BE	83.80±0.08	16.76	6.88	BE	82.91±2.37	33.91	11.63	88.75±2.14	29.22	8.97	BE	78.24±0.69	17.17	5.53
APD	97.94±0.02	0.25	0.16	APD	83.70±0.90	4.80	3.45	92.18±0.28	3.50	1.54	APD(*)	81.60±0.53	8.19	3.78
APDfix	97.99±0.01	0.10	0.11	APDfix	84.03±1.24	5.50	3.66	91.91±0.48	6.74	1.98	APDfix	78.14±0.12	6.53	2.63
GPM	96.69±0.02	0.45	0.27	GPM	87.27±0.61	4.54	1.88	88.52±0.28	6.97	2.82	GPM	80.41±0.16	28.33	13.02
WSN	97.91±0.02	0.36	0.22	WSN	86.74±0.40	8.54	2.89	92.58±0.39	4.62	1.21	WSN	82.55±0.44	17.09	7.57
BMKP	97.08±0.01	3.21	1.04	BMKP	84.03±0.55	9.32	3.07	92.57±0.65	9.08	2.13	BMKP	81.12±2.71	26.53	16.17
CLR	88.55±0.20	14.97	7.88	CLR	86.68±1.41	19.78	7.08	90.04±1.04	14.05	4.51	CLR	72.75±1.41	24.30	12.27
PRD	83.16±0.17	7.91	6.16	PRD	74.74±0.69	17.53	9.23	88.45±0.93	14.17	5.37	PRD	74.49±2.78	49.17	18.44
HALRP	98.10±0.03	0.47	0.24	HALRP	88.81±0.31	4.28	1.31	93.39±0.30	4.39	1.27	HALRP	83.08±0.73	10.36	3.91

(a) Results on P-MNIST.

(b) Results on Five-dataset with different backbones.

(c) Results on Omniglot.

Method	TinyImageNet 20-split						TinyImageNet 40-split					
	AlexNet			ResNet18			AlexNet			ResNet18		
	Acc.↑	MODP↓	AOPD↓	Acc.↑	MODP↓	AOPD↓	Acc.↑	MODP↓	AOPD↓	Acc.↑	MODP↓	AOPD↓
STL	66.78±0.18	6.20	3.43	67.00±0.30	5.87	2.87	74.65±0.17	8.16	4.36	74.08±0.25	8.13	4.08
MTL	71.23±0.54	6.87	3.42	73.64±0.46	6.94	3.31	78.80±0.25	7.74	3.92	80.05±0.22	9.07	4.04
L2	56.33±0.22	11.93	5.72	60.80±0.56	8.27	4.23	63.47±1.35	16.27	7.42	65.59±1.03	14.80	7.00
EWC	56.55±0.22	10.93	5.53	60.88±0.56	7.54	4.63	64.11±1.36	17.87	6.91	66.54±0.94	14.67	6.99
BN	57.20±0.11	12.07	5.37	61.03±0.65	9.73	4.24	64.04±1.15	19.07	7.23	66.17±1.75	15.33	6.92
BE	57.62±0.41	11.80	4.98	61.52±0.68	7.00	4.09	64.70±1.08	23.47	6.97	66.77±1.61	16.94	7.07
APD	67.26±0.38	12.00	5.43	68.76±0.58	9.86	4.33	73.88±0.46	8.53	5.04	73.85±0.40	11.46	5.57
APDfix	63.59±0.25	5.40	3.68	67.69±0.41	6.54	3.64	67.91±1.33	23.47	8.95	58.11±2.11	26.93	11.70
GPM	60.84±0.32	11.00	4.44	48.09±1.07	9.27	4.80	70.14±0.38	10.90	4.52	43.40±7.68	48.80	38.80
WSN	65.73±0.21	5.06	3.31	68.27±0.47	8.40	4.52	73.46±1.27	8.00	4.23	75.29±0.46	12.27	4.75
BMKP	65.01±0.41	5.87	3.37	67.45±0.59	10.60	6.69	73.57±0.21	9.60	4.31	74.84±0.63	12.90	4.95
CLR	57.29±0.39	8.80	4.42	61.77±0.47	10.27	5.42	65.22±0.49	9.86	5.74	67.59±0.92	16.54	9.30
PRD	46.49±0.30	15.40	8.33	49.65±0.57	19.33	11.59	53.54±0.45	19.74	10.02	63.78±0.50	20.27	7.93
HALRP	66.68±0.20	5.60	3.43	70.09±0.29	4.67	3.20	74.01±0.25	7.47	4.12	75.53±0.50	7.87	4.48

(d) Results on TinyImagenet with different backbones.

TABLE 3: Performance on P-MNIST, Five-dataset, Omniglot-Rotation and TinyImageNet. We ran experiments with five different task orders generated by different seeds on first two datasets. As for Omniglot-Rotation, we follow [19] to show the scalability under the original sequential order. Acc.↑ refers to the empirical accuracy, MOPD↓ and AOPD↓ refer to the task order robustness as discussed in Section 5.3. Results with * are from [9].

	PMNIST-20 (MLP)	CIFAR100-20 (ResNet18)	CIFAR100-20 (MLP)
Multitask(*)	96.8	70.2	16.4
IRU(*)	85.60 ± 0.15	68.46 ± 2.52	65.90 ± 2.16
Ours	92.02 ± 0.04	73.71 ± 0.87	67.21 ± 0.68

TABLE 4: Accuracies under the IRU [33] setting. Results with * are reported in [33].

results over five different task orders. The results on MOPD and AOPD on P-MNIST, Five-dataset, Omniglot-Rotation, TinyImageNet, and CIFAR100-Splits/-SuperClass are reported in Table 3a, Table 3b, Table 3c, Table 3d and Table 5, respectively. According to these results, we can generally conclude that our method can achieve a better accuracy-robustness trade-off, compared to the recent baseline APD.

5.4 Handling the Catastrophic Forgetting

We then evaluated the abilities of different methods for overcoming catastrophic forgetting. We illustrate the average forgetting (BWT) on the CIFAR100 Split/SuperClass dataset under different amounts of data in Fig. 2. Our proposed method can effectively address the forgetting issue, comparable with some state-of-the-art methods like WSN. We further provide detailed forgetting statistics within five different task orders in Appendix E.2.

5.5 Model Increment Analysis

Another potential issue in continual learning is the model size growth as the number of tasks increases. To compare increased model capacities among different methods, we visualize *the ratio of increased parameters* w.r.t to base model on the sequential 20 tasks of CIFAR100-SuperClass dataset in Fig. 3a. We can observe that our proposed HALRP can better control the model capacity increment. After the first four tasks, the model parameters are increased by around 19% and grow slowly during the last sixteen tasks (finally $\leq 28\%$). In contrast, the model parameters of APD grew quickly by around 40% in the first two or three tasks and kept a high ratio during the following tasks.

5.6 Computational Efficiency

We visualize the average time complexity ratio on the ten tasks of the PMNIST dataset in Fig. 3b. The time complexity ratio is computed by dividing the accumulated time across the tasks w.r.t. the time cost on the first task of single-task learning. We observe that our proposed method is also computationally efficient with limited time consumption compared to most baselines, with a better trade-off between performance and efficiency. Especially, our method needs less training time compared to WSN, BMKP and APD.

The major reason that should account for the inefficiency of WSN is that this method needs to optimize a weight

Method	CIFAR100-Split (with LeNet)								CIFAR100-SuperClass (with LeNet)							
	5%		25%		50%		100%		5%		25%		50%		100%	
	MOPD↓	AOPD↓	MOPD↓	AOPD↓	MOPD↓	AOPD↓	MOPD↓	AOPD↓	MOPD↓	AOPD↓	MOPD↓	AOPD↓	MOPD↓	AOPD↓	MOPD↓	AOPD↓
STL	1.96	1.38	3.44	2.41	3.68	2.57	4.38	3.13	2.52	1.48	3.64	1.44	2.52	1.48	2.64	1.45
MTL	1.44	0.93	1.34	0.87	1.66	0.71	1.54	0.84	6.96	2.66	12.04	4.89	13.96	5.74	13.48	6.29
L2	11.66	6.13	13.14	6.96	15.02	7.50	15.18	7.15	9.92	4.55	13.24	6.43	13.32	7.04	14.44	6.82
EWC	11.92	6.07	13.20	6.85	13.78	6.96	13.44	6.48	13.24	5.60	10.92	6.53	13.48	8.03	21.60	8.32
BN	11.70	5.95	13.28	7.37	12.40	6.91	13.92	7.90	8.52	3.35	11.20	3.99	11.64	4.05	11.40	4.25
BE	12.12	5.47	12.92	6.13	9.28	5.56	8.50	5.35	9.56	3.46	11.88	4.00	11.80	3.88	10.84	4.03
APD	11.42	7.21	6.48	3.77	8.00	4.10	8.88	4.07	26.56	12.98	8.64	4.39	8.28	4.48	6.72	3.26
APDfix	6.64	4.39	8.32	4.94	8.92	5.54	7.40	4.21	9.04	4.90	10.28	5.68	8.56	5.32	6.04	2.70
IBPWF	4.30	2.84	4.60	2.73	5.40	3.07	3.68	2.68	14.84	7.45	4.44	2.45	5.36	2.86	5.52	3.38
GPM	11.14	6.37	6.32	4.22	6.32	3.69	2.28	1.348	9.32	4.46	10.00	5.53	8.84	5.89	7.68	4.47
WSN	4.16	2.57	4.42	2.71	4.2	2.62	3.56	2.39	5.08	3.14	4.76	3.192	4.00	2.16	3.76	2.36
BMKP	12.98	7.63	13.22	6.50	6.52	4.30	8.34	3.35	11.72	6.03	13.32	5.27	11.08	4.43	3.72	1.99
CLR	13.50	7.14	12.77	6.13	8.90	5.82	9.37	5.34	10.00	4.01	7.67	3.84	6.60	3.71	9.00	4.06
PRD	5.80	3.80	4.60	2.66	4.16	2.63	5.20	3.16	7.47	4.28	8.33	3.95	5.33	3.29	5.00	2.86
HALRP	2.56	1.34	2.58	1.44	2.34	1.71	3.90	2.56	2.96	1.65	3.40	1.91	4.48	1.65	4.34	1.96

TABLE 5: Task order robustness evaluation on CIFAR100-Split/SuperClass with different amounts of training data.

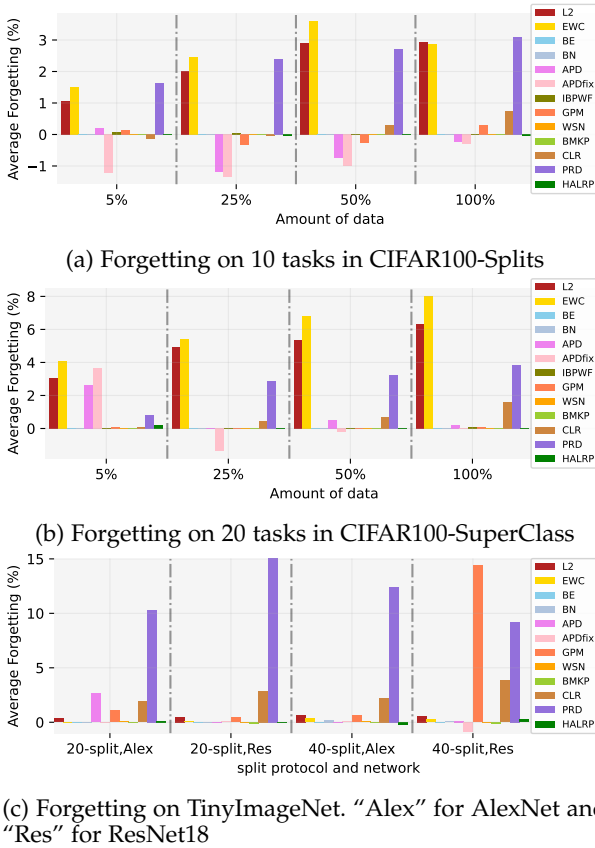


Fig. 2: Average Forgetting Statistics

score for each model parameter and then generate binary masks by locating a certain sparsity quantile among the weight scores in each layer, which is very time-consuming. Especially, we can observe a non-linear increase in behavior for BMKP and APD in Fig. 3b. In BMKP, the pattern basis of the core knowledge space increases along the sequential tasks and then the knowledge projection between two memory levels will cost more time as the tasks pass. A severe drawback of APD method is that when the task t arrives for learning, it needs to recover the parameters θ_i^* for all previous tasks $i = 0, 1, \dots, t-1$ and then apply the regularization $\sum_{i=0}^{t-1} \|\theta_t - \theta_i^*\|_2^2$ between the weights of current task (i.e., θ_t) and each previous task (i.e., θ_i^*). This

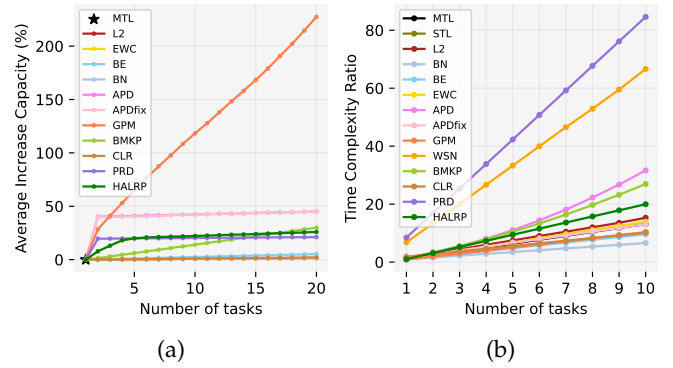


Fig. 3: (a) Average Capacity Increment ratio on CIFAR100-SuperClass w.r.t. the base model. (b) Average Time Complexity Ratio on PMNIST.

defect becomes more time-consuming as more tasks arrive. Besides, an extra k -means clustering process is needed for the hierarchical knowledge consolidation among tasks in APD. The difference of computational efficiency becomes more significant on the challenging scenarios with more tasks and complex network architectures. As for PRD, it is inefficient as this method converges slower than other methods, due to the reason that it adopted supervised contrastive loss instead of cross-entropy loss.

Apart from the time efficiency, we also tracked the GPU memory usage during the training. The results showed that our method only requires limited GPU memory for training compared to other state-of-the-art methods. See Appendix E.3 for more details.

5.7 Ablation Studies

In this part, we provide ablation studies about some hyperparameters in our method.

Ablation study about the rank selection We report the additional studies to evaluate the impacts of the hyperparameters selection on the rank selection process. We conduct the following ablations: (1) varying the warm-up epochs n_r , (2) varying the loss approximation rate α , (3) **LRP**: omitting the importance estimation (step 6 of Algorithm 1), and (4) **Random LRP**: replacing step 6 of Algorithm 1 with a random decomposition. The relevant results on CIFAR100-Splits are depicted in Table 6. We can

Ablation	Acc.↑	Size↓
$\alpha: 0.9, n_r: 1$	68.39 ± 0.13	0.234
$\alpha: 0.9, n_r: 2$	67.93 ± 0.19	0.234
$\alpha: 0.9, n_r: 3$	67.38 ± 0.12	0.234
$\alpha: 0.9, n_r: 4$	67.04 ± 0.08	0.234
$\alpha: 0.95, n_r: 1$	68.09 ± 0.15	0.234
$\alpha: 0.75, n_r: 1$	68.26 ± 0.11	0.217
$\alpha: 0.60, n_r: 1$	66.87 ± 0.23	0.165
$\alpha: 0.45, n_r: 1$	66.08 ± 0.14	0.100
LRP.	67.49 ± 0.13	0.234
Random LRP.	61.76 ± 0.18	0.235

TABLE 6: Ablation studies. Acc.↑ refers to the accuracy; Size refers to the relative increment size.

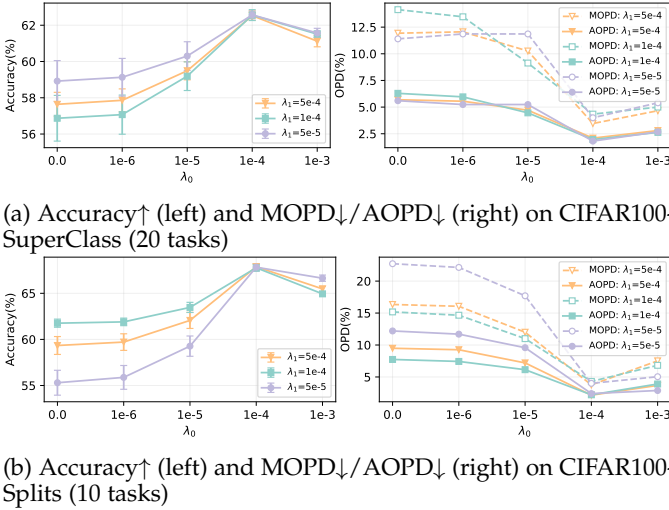


Fig. 4: Effect of regularization coefficients λ_0 and λ_1 .

observe that the performance will not significantly rise as n_r increases, which indicates that only one epoch is enough for warm-up training. When decreasing the approximate rate α , the accuracy will decay. Furthermore, if we apply the random decomposition of the model, the accuracy will sharply drop, indicating the necessity of our Hessian aware-decomposition procedure.

Effect of the regularization coefficients λ_0 and λ_1
 To investigate the effects of the regularization coefficients introduced in Eq. 12, we further conducted experiments on two datasets: CIFAR100-SuperClass and CIFAR100-Splits. We adopted values from $\{0, 1e-6, 1e-5, 1e-4, 1e-3\}$ for λ_0 and $\{5e-4, 1e-4, 5e-5\}$ for λ_1 . For each combination, we reported MOPD/AOPD for task order robustness as well as the average accuracy on the above two datasets, and the results are illustrated in Fig. 4. We can see that the regularization coefficients λ_0 and λ_1 have potential effects on the final accuracy and task order robustness. In our experiments, we choose the optimal hyperparameters by validation. Furthermore, some selected hyperparameters are also applied to realize fair comparisons, e.g., we set L_2 -regularizer coefficient $\lambda_1 = 1e-4$ for all other methods on CIFAR100-SuperClass and CIFAR100-Splits. See Appendix F.3 for more details.

6 CONCLUSION

In this work, we propose a low-rank perturbation method for continual learning. Specifically, we approximate the task-adaptive parameters with low-rank decomposition by formulating the model transition along the sequential tasks with parameter transformations. We theoretically show the quantitative relationship between the Hessian and the proposed low-rank approximation, which leads to a novel Hessian-aware framework that enables the model to automatically select ranks by the relevant importance of the perturbation to the model’s performance. The extensive experimental results show that our proposed method performs better on the robustness of different task orders and the ability to address catastrophic forgetting issues.

ACKNOWLEDGMENTS

The work of Fan Zhou, Rui Wang and Shichun Yang is supported by the National Natural Science Foundation of China, Young Scientist Fund (52302487). Jiaqi Li, Yuanhao Lai, Sabyasachi Sahoo, Charles X. Ling, Boyu Wang and Christian Gagné are supported in part by the Science and the Natural Sciences and Engineering Research Council of Canada (NSERC), in part by the NSERC Discovery Grants Program.

REFERENCES

- [1] M. De Lange, R. Aljundi, M. Masana, S. Parisot, X. Jia, A. Leonardis, G. Slabaugh, and T. Tuytelaars, “A continual learning survey: Defying forgetting in classification tasks,” *IEEE transactions on pattern analysis and machine intelligence*, vol. 44, no. 7, pp. 3366–3385, 2021.
- [2] G. Saha, I. Garg, and K. Roy, “Gradient projection memory for continual learning,” in *International Conference on Learning Representations*, 2021.
- [3] M. Farajtabar, N. Azizan, A. Mott, and A. Li, “Orthogonal gradient descent for continual learning,” in *International Conference on Artificial Intelligence and Statistics*. PMLR, 2020, pp. 3762–3773.
- [4] J. Kirkpatrick, R. Pascanu, N. Rabinowitz, J. Veness, G. Desjardins, A. A. Rusu, K. Milan, J. Quan, T. Ramalho, A. Grabska-Barwinska et al., “Overcoming catastrophic forgetting in neural networks,” *Proceedings of the national academy of sciences*, vol. 114, no. 13, pp. 3521–3526, 2017.
- [5] S. Jung, H. Ahn, S. Cha, and T. Moon, “Continual learning with node-importance based adaptive group sparse regularization,” *Advances in Neural Information Processing Systems*, vol. 33, pp. 3647–3658, 2020.
- [6] M. K. Titsias, J. Schwarz, A. G. d. G. Matthews, R. Pascanu, and Y. W. Teh, “Functional regularisation for continual learning with gaussian processes,” *arXiv preprint arXiv:1901.11356*, 2019.
- [7] S. Wang, X. Li, J. Sun, and Z. Xu, “Training networks in null space of feature covariance for continual learning,” in *Proceedings of the IEEE/CVF conference on Computer Vision and Pattern Recognition*, 2021, pp. 184–193.
- [8] Y. Kong, L. Liu, H. Chen, J. Kacprzyk, and D. Tao, “Overcoming catastrophic forgetting in continual learning by exploring eigenvalues of hessian matrix,” *IEEE Transactions on Neural Networks and Learning Systems*, pp. 1–15, 2023.
- [9] J. Yoon, S. Kim, E. Yang, and S. J. Hwang, “Scalable and order-robust continual learning with additive parameter decomposition,” in *8th International Conference on Learning Representations, ICLR 2020, Addis Ababa, Ethiopia, April 26-30, 2020*, 2020.
- [10] N. Mehta, K. Liang, V. K. Verma, and L. Carin, “Continual learning using a bayesian nonparametric dictionary of weight factors,” in *International Conference on Artificial Intelligence and Statistics*. PMLR, 2021, pp. 100–108.
- [11] Y. Wen, D. Tran, and J. Ba, “Batchensemble: an alternative approach to efficient ensemble and lifelong learning,” in *8th International Conference on Learning Representations, ICLR 2020, Addis Ababa, Ethiopia, April 26-30, 2020*. OpenReview.net, 2020.

- [12] A. Chaudhry, N. Khan, P. Dokania, and P. Torr, "Continual learning in low-rank orthogonal subspaces," *Advances in Neural Information Processing Systems*, vol. 33, pp. 9900–9911, 2020.
- [13] Y. Yang, Z.-Q. Sun, H. Zhu, Y. Fu, Y. Zhou, H. Xiong, and J. Yang, "Learning adaptive embedding considering incremental class," *IEEE Transactions on Knowledge and Data Engineering*, vol. 35, no. 3, pp. 2736–2749, 2023.
- [14] A. A. Rusu, N. C. Rabinowitz, G. Desjardins, H. Soyer, J. Kirkpatrick, K. Kavukcuoglu, R. Pascanu, and R. Hadsell, "Progressive neural networks," *arXiv preprint arXiv:1606.04671*, 2016.
- [15] J. Yoon, E. Yang, J. Lee, and S. J. Hwang, "Lifelong learning with dynamically expandable networks," in *Proceedings of International Conference on Learning Representations*, 2017.
- [16] X. Li, Y. Zhou, T. Wu, R. Socher, and C. Xiong, "Learn to grow: A continual structure learning framework for overcoming catastrophic forgetting," in *International Conference on Machine Learning*. PMLR, 2019, pp. 3925–3934.
- [17] A.-A. Liu, H. Lu, H. Zhou, T. Li, and M. Kankanhalli, "Balanced class-incremental 3d object classification and retrieval," *IEEE Transactions on Knowledge and Data Engineering*, pp. 1–13, 2023.
- [18] Y. Ge, Y. Li, S. Ni, J. Zhao, M.-H. Yang, and L. Itti, "Clr: Channel-wise lightweight reprogramming for continual learning," in *Proceedings of the IEEE/CVF International Conference on Computer Vision*, 2023, pp. 18798–18808.
- [19] H. Kang, R. J. L. Mina, S. R. H. Madjid, J. Yoon, M. Hasegawa-Johnson, S. J. Hwang, and C. D. Yoo, "Forget-free continual learning with winning subnetworks," in *International Conference on Machine Learning*. PMLR, 2022, pp. 10734–10750.
- [20] M. Riemer, I. Cases, R. Ajemian, M. Liu, I. Rish, Y. Tu, and G. Tesauro, "Learning to learn without forgetting by maximizing transfer and minimizing interference," *arXiv preprint arXiv:1810.11910*, 2018.
- [21] S.-A. Rebuffi, A. Kolesnikov, G. Sperl, and C. H. Lampert, "icarl: Incremental classifier and representation learning," in *Proceedings of the IEEE conference on Computer Vision and Pattern Recognition*, 2017, pp. 2001–2010.
- [22] B. Zhang, Y. Guo, Y. Li, Y. He, H. Wang, and Q. Dai, "Memory recall: A simple neural network training framework against catastrophic forgetting," *IEEE Transactions on Neural Networks and Learning Systems*, vol. 33, no. 5, pp. 2010–2022, 2022.
- [23] H. Chen, Y. Wang, and Q. Hu, "Multi-granularity regularized rebalancing for class incremental learning," *IEEE Transactions on Knowledge and Data Engineering*, vol. 35, no. 7, pp. 7263–7277, 2023.
- [24] G. Sun, Y. Cong, Y. Zhang, G. Zhao, and Y. Fu, "Continual multiview task learning via deep matrix factorization," *IEEE Transactions on Neural Networks and Learning Systems*, vol. 32, no. 1, pp. 139–150, 2021.
- [25] S. Ho, M. Liu, L. Du, L. Gao, and Y. Xiang, "Prototype-guided memory replay for continual learning," *IEEE Transactions on Neural Networks and Learning Systems*, 2023.
- [26] L. Wang, B. Lei, Q. Li, H. Su, J. Zhu, and Y. Zhong, "Triple-memory networks: A brain-inspired method for continual learning," *IEEE Transactions on Neural Networks and Learning Systems*, vol. 33, no. 5, pp. 1925–1934, 2021.
- [27] A. Chaudhry, M. Ranzato, M. Rohrbach, and M. Elhoseiny, "Efficient lifelong learning with a-gem," *International Conference on Learning Representations*, 2019.
- [28] C. Tai, T. Xiao, X. Wang, and W. E, "Convolutional neural networks with low-rank regularization," in *4th International Conference on Learning Representations, ICLR 2016, San Juan, Puerto Rico, May 2–4, 2016, Conference Track Proceedings*, Y. Bengio and Y. LeCun, Eds., 2016.
- [29] Y. Idelbayev and M. A. Carreira-Perpinán, "Low-rank compression of neural nets: Learning the rank of each layer," in *Proceedings of the IEEE/CVF Conference on Computer Vision and Pattern Recognition*, 2020, pp. 8049–8059.
- [30] A.-H. Phan, K. Sobolev, K. Sozykin, D. Ermilov, J. Gusak, P. Tichavský, V. Glukhov, I. Oseledets, and A. Cichocki, "Stable low-rank tensor decomposition for compression of convolutional neural network," in *European Conference on Computer Vision*. Springer, 2020, pp. 522–539.
- [31] L. Wang, M. Rege, M. Dong, and Y. Ding, "Low-rank kernel matrix factorization for large-scale evolutionary clustering," *IEEE Transactions on Knowledge and Data Engineering*, vol. 24, no. 6, pp. 1036–1050, 2012.
- [32] X. Zhu, S. Zhang, Y. Li, J. Zhang, L. Yang, and Y. Fang, "Low-rank sparse subspace for spectral clustering," *IEEE Transactions on Knowledge and Data Engineering*, vol. 31, no. 8, pp. 1532–1543, 2019.
- [33] R. Hyder, K. Shao, B. Hou, P. Markopoulos, A. Prater-Bennette, and M. S. Asif, "Incremental task learning with incremental rank updates," in *European Conference on Computer Vision*. Springer, 2022, pp. 566–582.
- [34] C. Eckart and G. Young, "The approximation of one matrix by another of lower rank," *Psychometrika*, vol. 1, no. 3, pp. 211–218, 1936.
- [35] C. R. Harris, K. J. Millman, S. J. van der Walt, R. Gommers, P. Virtanen, D. Cournapeau, E. Wieser, J. Taylor, S. Berg, N. J. Smith, R. Kern, M. Picus, S. Hoyer, M. H. van Kerkwijk, M. Brett, A. Haldane, J. F. del Río, M. Wiebe, P. Peterson, P. Gérard-Marchant, K. Sheppard, T. Reddy, W. Weckesser, H. Abbasi, C. Gohlke, and T. E. Oliphant, "Array programming with NumPy," *Nature*, vol. 585, no. 7825, pp. 357–362, Sep. 2020.
- [36] A. Paszke, S. Gross, S. Chintala, G. Chanan, E. Yang, Z. DeVito, Z. Lin, A. Desmaison, L. Antiga, and A. Lerer, "Automatic differentiation in pytorch," 2017.
- [37] Z. Dong, Z. Yao, A. Gholami, M. W. Mahoney, and K. Keutzer, "Hawq: Hessian aware quantization of neural networks with mixed-precision," in *Proceedings of the IEEE/CVF International Conference on Computer Vision*, 2019, pp. 293–302.
- [38] Z. Dong, Z. Yao, D. Arfeen, A. Gholami, M. W. Mahoney, and K. Keutzer, "Hawq-v2: Hessian aware trace-weighted quantization of neural networks," *Advances in neural information processing systems*, vol. 33, pp. 18518–18529, 2020.
- [39] F. Kunstner, P. Hennig, and L. Balles, "Limitations of the empirical fisher approximation for natural gradient descent," *Advances in neural information processing systems*, vol. 32, 2019.
- [40] S. Ebrahimi, M. Elhoseiny, T. Darrell, and M. Rohrbach, "Uncertainty-guided continual learning with bayesian neural networks," *arXiv preprint arXiv:1906.02425*, 2019.
- [41] A. Krizhevsky, G. Hinton *et al.*, "Learning multiple layers of features from tiny images," 2009.
- [42] L. Deng, "The mnist database of handwritten digit images for machine learning research," *IEEE Signal Processing Magazine*, vol. 29, no. 6, pp. 141–142, 2012.
- [43] Y. Bulatov, "Notmnist dataset. google (books/ocr)," Tech. Rep.[Online]. Available: <http://yaroslavvb.blogspot.it/2011/09...>, Tech. Rep., 2011.
- [44] H. Xiao, K. Rasul, and R. Vollgraf. (2017) Fashion-mnist: a novel image dataset for benchmarking machine learning algorithms.
- [45] N. Yuval, W. Tao, C. Adam, B. Alessandro, W. Bo, and N. Andrew Y., "Reading digits in natural images with unsupervised feature learning," in *In Proceedings of NIPS Workshop on Deep Learning and Unsupervised Feature Learning*. PMLR, 2011, pp. 522–539.
- [46] B. M. Lake, R. Salakhutdinov, and J. B. Tenenbaum, "Human-level concept learning through probabilistic program induction," *Science*, vol. 350, no. 6266, pp. 1332–1338, 2015.
- [47] J. Deng, W. Dong, R. Socher, L.-J. Li, K. Li, and L. Fei-Fei, "Imagenet: A large-scale hierarchical image database," in *2009 IEEE conference on computer vision and pattern recognition*. Ieee, 2009, pp. 248–255.
- [48] Y. Zhang and Q. Yang, "A survey on multi-task learning," *IEEE Transactions on Knowledge and Data Engineering*, vol. 34, no. 12, pp. 5586–5609, 2022.
- [49] S. Ioffe and C. Szegedy, "Batch normalization: Accelerating deep network training by reducing internal covariate shift," in *International conference on machine learning*. PMLR, 2015, pp. 448–456.
- [50] W. Sun, Q. Li, J. Zhang, W. Wang, and Y.-a. Geng, "Decoupling learning and remembering: A bilevel memory framework with knowledge projection for task-incremental learning," in *Proceedings of the IEEE/CVF Conference on Computer Vision and Pattern Recognition*, 2023, pp. 20186–20195.
- [51] N. Asadi, M. Davari, S. Mudur, R. Aljundi, and E. Belilovsky, "Prototype-sample relation distillation: towards replay-free continual learning," in *International Conference on Machine Learning*. PMLR, 2023, pp. 1093–1106.
- [52] V. K. Verma, K. J. Liang, N. Mehta, P. Rai, and L. Carin, "Efficient feature transformations for discriminative and generative continual learning," in *Proceedings of the IEEE/CVF Conference on Computer Vision and Pattern Recognition*, 2021, pp. 13865–13875.

APPENDIX A

BACKGROUND ON LOW-RANK FACTORIZATION FOR MATRIX

Here, we provide more background knowledge about the low-rank matrix factorization.

In this work, we leverage the Eckart–Young–Mirsky theorem [34] with the Frobenius norm. In this part, we provide background knowledge for the self-cohesion of the paper.

Denote by $\mathbf{B} \in \mathbb{R}^{m \times n}$ a real (possibly rectangular) matrix. Suppose that $\mathbf{B} = \mathbf{U}\Sigma\mathbf{V}^\top$ is the singular value decomposition (SVD) of \mathbf{B} , then, we can claim that the best rank k approximation ($k \leq \min\{m, n\}$) to \mathbf{B} under the Frobenius norm $\|\cdot\|_F$ is given by $\mathbf{B}_k = \sum_{i=1}^k \sigma_i \mathbf{u}_i \mathbf{v}_i^\top$, where \mathbf{u}_i and \mathbf{v}_i denote the i^{th} column of \mathbf{U} and \mathbf{V} , respectively. Then,

$$\|\mathbf{B} - \mathbf{B}_k\|_F^2 = \left\| \sum_{i=k+1}^n \sigma_i \mathbf{u}_i \mathbf{v}_i^\top \right\|_F^2 = \sum_{i=k+1}^n \sigma_i^2$$

Thus, we need to show that if $\mathbf{A}_k = \mathbf{X}\mathbf{Y}^\top$ where \mathbf{X} and \mathbf{Y} has k columns

$$\|\mathbf{B} - \mathbf{B}_k\|_F^2 = \sum_{i=k+1}^n \sigma_i^2 \leq \|\mathbf{B} - \mathbf{A}_k\|_F^2$$

By the triangle inequality, if $\mathbf{B} = \mathbf{B}' + \mathbf{B}''$ then $\sigma_1(\mathbf{B}) \leq \sigma_1(\mathbf{B}') + \sigma_1(\mathbf{B}'')$. Denote by \mathbf{B}'_k and \mathbf{B}''_k the rank k approximation to \mathbf{B}' and \mathbf{B}'' by the SVD method, respectively. Then, for any $i, j \geq 1$,

$$\begin{aligned} \sigma_i(\mathbf{B}') + \sigma_j(\mathbf{B}'') &= \sigma_1(\mathbf{B}' - \mathbf{B}'_{i-1}) + \sigma_1(\mathbf{B}'' - \mathbf{B}''_{j-1}) \\ &\geq \sigma_1(\mathbf{B} - \mathbf{B}'_{i-1} - \mathbf{B}''_{j-1}) \\ &\geq \sigma_1(\mathbf{B} - \mathbf{B}_{i+j-2}) \\ &= \sigma_{i+j-1}(\mathbf{B}) \end{aligned}$$

where the last inequality comes from the fact that $\text{rank}(\mathbf{B}'_{i-1} + \mathbf{B}''_{j-1}) \leq \text{rank}(\mathbf{B}_{i+j-2})$.

Since $\sigma_{k+1}(\mathbf{B}_k) = 0$, when $\mathbf{B}' = \mathbf{B} - \mathbf{A}_k$ and $\mathbf{B}'' = \mathbf{A}_k$ we conclude that for $i \geq 1, j = k + 1$

$$\sigma_i(\mathbf{B} - \mathbf{A}_k) \geq \sigma_{k+i}(\mathbf{B})$$

Therefore,

$$\|\mathbf{B} - \mathbf{A}_k\|_F^2 = \sum_{i=1}^n \sigma_i(\mathbf{B} - \mathbf{A}_k)^2 \geq \sum_{i=k+1}^n \sigma_i(\mathbf{B})^2 = \|\mathbf{B} - \mathbf{B}_k\|_F^2$$

Thus, we can get Eq. 1 displayed in the paper.

APPENDIX B

PROOF TO THEOREM 1 AND DISCUSSION

Theorem 1. Assume that a neural network of L layers with vectorized weights $(\omega_1^*, \dots, \omega_L^*)$ that have converged to local optima, such that the first and second order optimality conditions are satisfied, i.e., the gradient is zero, and the Hessian is positive semi-definite. Suppose a perturbation $\Delta\omega_1^*$ applied to the first layer weights, then we have the loss increment

$$\begin{aligned} \mathcal{L}(\omega_1^* - \Delta\omega_1^*, \dots, \omega_L^*) - \mathcal{L}(\omega_1^*, \dots, \omega_L^*) \\ \leq \frac{1}{2} \mathbf{H}_1 \|\Delta\omega_1^*\|_F^2 + o(\|\Delta\omega_1^*\|_F^2), \end{aligned} \quad (15)$$

where $\mathbf{H}_1 = \Delta\mathcal{L}(\omega_1^*)$ is the Hessian matrix at only the variables of the first layer weights.

Proof. Denote the gradient and Hessian of the first layer ω_1^* as \mathbf{g}_1 and \mathbf{H}_1 . Through Taylor's expansion, we have

$$\begin{aligned} \mathcal{L}(\omega_1^* - \Delta\omega_1^*, \dots, \omega_L^*) - \mathcal{L}(\omega_1^*, \dots, \omega_L^*) \\ = -\mathbf{g}_1^T \Delta\omega_1^* + \frac{1}{2} \Delta\omega_1^{*T} \mathbf{H}_1 \Delta\omega_1^* + o(\|\Delta\omega_1^*\|_F^2). \end{aligned}$$

Using the fact that the gradient is zero at the local optimum ω_1^* as well as the sub-additive and sub-multiplicative properties of Frobenius norm, we have,

$$\begin{aligned} \mathcal{L}(\omega_1^* - \Delta\omega_1^*, \dots, \omega_L^*) - \mathcal{L}(\omega_1^*, \dots, \omega_L^*) \\ = \frac{1}{2} \Delta\omega_1^{*T} \mathbf{H}_1 \Delta\omega_1^* + o(\|\Delta\omega_1^*\|_F^2) \\ \leq \frac{1}{2} \Delta\omega_1^{*T} \mathbf{H}_1 \Delta\omega_1^* + o(\|\Delta\omega_1^*\|_F^2) \\ \leq \frac{1}{2} \Delta\omega_1^{*T} \mathbf{H}_1 \Delta\omega_1^* + o(\|\Delta\omega_1^*\|_F^2) \\ \leq \frac{1}{2} \|\mathbf{H}_1\|_F \|\Delta\omega_1^*\|_F^2 + o(\|\Delta\omega_1^*\|_F^2). \end{aligned}$$

Thus, we conclude the proof. \square

Algorithm 1 implies that the Hessian information can be used to quantitatively measure the influences of low-rank perturbation on the model's empirical losses. In practice, we can approximate the Hessian by the negative empirical Fisher information [39]. This enables a dynamic scheme for the trade-off between the approximation error and computational efficiency. For a given loss approximation rate, the model can automatically select the rank for all the layers.

APPENDIX C

SOLVING $\mathbf{R}^{\text{FREE}}, \mathbf{S}^{\text{FREE}}, \mathbf{B}^{\text{FREE}}$

In Section 4.1, we described that when a new task comes, we first train the model on it for several epochs. With this step, we can obtain a rough parameter estimation \mathbf{W}^{free} of this new task, which indicates the freely-trained weights without any constraints. Then, we can obtain $\mathbf{R}^{\text{free}}, \mathbf{S}^{\text{free}}, \mathbf{B}^{\text{free}}$ by solving the following problem:

$$\mathbf{R}^{\text{free}} = \arg \min_{\mathbf{R}} \|\mathbf{W}^{\text{free}} - \mathbf{R}\mathbf{W}^{\text{base}}\|_F^2 \quad (16)$$

$$\mathbf{S}^{\text{free}} = \arg \min_{\mathbf{S}} \|\mathbf{W}^{\text{free}} - \mathbf{R}^{\text{free}}\mathbf{W}^{\text{base}}\mathbf{S}\|_F^2 \quad (17)$$

$$\mathbf{B}^{\text{free}} = \mathbf{W}^{\text{free}} - \mathbf{R}^{\text{free}}\mathbf{W}^{\text{base}}\mathbf{S}^{\text{free}} \quad (18)$$

Simply, $\|\mathbf{W}^{\text{free}} - \mathbf{R}\mathbf{W}^{\text{base}}\|_F^2 = \sum_{i=1}^I \sum_{j=1}^J (w_{ji}^{\text{free}} - r_j w_{ji}^{\text{base}})^2$, where w_{ji}^{free} and w_{ji}^{base} are the elements of j -th row and i -th column of \mathbf{W}^{free} and \mathbf{W}^{base} , respectively. By taking the derivative of the above expression w.r.t. r_j and let it equals 0, we can obtain:

$$r_j^{\text{free}} = \frac{\sum_{i=1}^I w_{ji}^{\text{free}} w_{ji}^{\text{base}}}{\sum_{i=1}^I (w_{ji}^{\text{base}})^2} \quad (19)$$

Similarly, $\|\mathbf{W}^{\text{free}} - \mathbf{R}^{\text{free}}\mathbf{W}^{\text{base}}\mathbf{S}\|_F^2 = \sum_{i=1}^I \sum_{j=1}^J (w_{ji}^{\text{free}} - r_j^{\text{free}} w_{ji}^{\text{base}} s_i)^2$. By taking the derivative w.r.t. s_i and let it equals 0, we can obtain:

$$s_i^{\text{free}} = \frac{\sum_{j=1}^J r_j^{\text{free}} w_{ji}^{\text{free}} w_{ji}^{\text{base}}}{\sum_{j=1}^J (r_j^{\text{free}} w_{ji}^{\text{base}})^2} \quad (20)$$

Then, we can calculate \mathbf{B}^{free} by the third equation using the obtained \mathbf{R}^{free} and \mathbf{S}^{free} .

Finally, the low rank approximation can be applied on \mathbf{W}^{free} with SVD:

$$\mathbf{W}^{\text{free}} \approx \mathbf{W}^{(k)\text{free}} = \mathbf{R}^{\text{free}} \mathbf{W}^{\text{base}} \mathbf{S}^{\text{free}} + \mathbf{B}^{(k)\text{free}}, \quad (21)$$

where $\mathbf{B}^{(k)\text{free}} = \mathbf{U}^{(k)\text{free}} \mathbf{\Sigma}^{(k)\text{free}} (\mathbf{V}^{(k)\text{free}})^\top$.

Note that the number of parameters in the original weights $\mathbf{W}^{\text{free}} \in \mathbb{R}^{J \times I}$ is $\text{size}\{\mathbf{W}^{\text{free}}\} = JI$. After this approximation, we only need to store the weights \mathbf{R}^{free} , \mathbf{S}^{free} , $\mathbf{U}^{(k)\text{free}}$, $\mathbf{\Sigma}^{(k)\text{free}}$, $\mathbf{V}^{(k)\text{free}}$ for a new task, whose parameter number is $\text{size}\{\mathbf{R}^{\text{free}}, \mathbf{S}^{\text{free}}, \mathbf{U}^{(k)\text{free}}, \mathbf{\Sigma}^{(k)\text{free}}, \mathbf{V}^{(k)\text{free}}\} = J + I + kJ + k + kI = (J+I)(k+1) + k$. Thus, the incremental ratio is $\rho = \frac{(J+I)(k+1)+k}{JI} \ll 1$ in practice.

APPENDIX D

DISCUSSION ON THE FINE-TUNING OBJECTIVE ON THE NEW TASK

In the proposed algorithm, we finally fine-tune the model on the new task with Eq. 12 in the manuscript, which is re-illustrated below,

$$\min_{\mathbf{W}_t} \mathcal{L}(\mathbf{W}_t; \mathcal{D}_t) + \mathcal{L}_{\text{reg}}(\mathbf{W}_t) \quad (22)$$

where

$$\begin{aligned} \mathcal{L}_{\text{reg}}(\mathbf{W}_t) = & \sum_l \left[\underbrace{\lambda_0 (\|\mathbf{U}_i^{(k_l)\text{free}}\| + \|\mathbf{V}_i^{(k_l)\text{free}}\|)}_{L_1\text{-regularization}} \right. \\ & \left. + \lambda_1 (\underbrace{\|\mathbf{R}_i^{\text{free}}\|_2^2 + \|\mathbf{S}_i^{\text{free}}\|_2^2 + \|\mathbf{U}_i^{(k_l)\text{free}}\|_2^2 + \|\mathbf{V}_i^{(k_l)\text{free}}\|_2^2}_{L_2\text{-regularization}}) \right] \end{aligned} \quad (23)$$

The fine-tuning objective mainly consists of three parts, the general cross-entropy loss on the new task \mathcal{T}_t , a L_1 regularization term on $\|\mathbf{U}_i^{(k_l)\text{free}}\| + \|\mathbf{V}_i^{(k_l)\text{free}}\|$, and the L_2 regularization terms on $\|\mathbf{R}_i^{\text{free}}\|_2^2 + \|\mathbf{S}_i^{\text{free}}\|_2^2$ and $\|\mathbf{U}_i^{(k_l)\text{free}}\|_2^2 + \|\mathbf{V}_i^{(k_l)\text{free}}\|_2^2$, respectively.

As mentioned in the paper, we apply the L_1 regularization on $\mathbf{U}_i^{(k_l)\text{free}}$ and $\mathbf{V}_i^{(k_l)\text{free}}$. Besides, as discussed in Section 4.4 of the paper, we also apply to prune $\mathbf{U}_i^{\text{free}}$ and $\mathbf{V}_i^{(k_l)\text{free}}$, which further encouraged the sparsity.

Our method keeps \mathbf{W}^{base} as unchanged for new tasks for knowledge transfer, while the $\mathbf{R}_i^{\text{free}}$, $\mathbf{S}_i^{\text{free}}$, $\mathbf{U}_i^{(k)\text{free}}$ and $\mathbf{V}_i^{(k)\text{free}}$ are left as task-adaptive parameters. Since $\mathbf{R}_i^{\text{free}}$ and $\mathbf{S}_i^{\text{free}}$ are diagonal matrices, plus the fact that $\mathbf{U}_i^{(k)\text{free}}$ and $\mathbf{V}_i^{(k)\text{free}}$ are sparse, thus the model only needs to learn a small number of parameters. Unlike some regularization methods (e.g. EWC [4]), which constrain the gradient update and require to re-train a lot of parameters, our method can update the model more efficiently. In addition, the empirical results reported in the paper show that our method can also achieve better performance with less time and memory cost.

APPENDIX E

ADDITIONAL EXPERIMENTAL RESULTS

E.1 Comparing with other low-rank methods

Our work also shares some similarities with the low-rank-decomposition-based method IBPWF [10]. As discussed

	P-MNIST		
	Acc.↑	MOPD↓	AOPD↓
IBPWF	78.12 ± 0.83	12.69	6.65
HALRP	98.10 ± 0.03	0.47	0.24
	Five-dataset		
	Acc.↑	MOPD↓	AOPD↓
IBPWF	84.62 ± 0.36	5.06	1.72
HALRP	88.81 ± 0.31	4.28	1.31

TABLE 7: Comparison with low-rank factorization method

in [33] and in our paper (Sec. 1), this method requires larger ranks to accept higher accuracy. Furthermore, as pointed out by [52], IBPWF leverages Bayesian non-parametric to let the data dictate expansion, but the benchmarks considered in Bayesian methods have been limited to smaller datasets, like MNIST and CIFAR-10. In addition to the experimental comparisons with IBPWF reported in the paper, we further report more results in Table 7. We can observe that our method outperforms IBPWF with a large gap in terms of Accuracy and MOPD↓ & AOPD↓. Furthermore, we observe that IBPWF cannot perform well on P-MNIST, which is 10× the number of data of MNIST. The gap is consistent with observations in [52].

E.2 Performance on Alleviate Forgetting on Different Task Orders

In the main paper, we report the forgetting performance on the average of five task orders (A-E) on CIFAR100 Splits and SuperClass. In this part, we provide the performance on forgetting under each task order in Fig. 5 and Fig. 6, under different amounts (i.e., 5% ~ 100%) of training data from.

E.3 Analysis of Memory Overhead

We also provided some quantitative results to support the memory efficiency of our proposed HALRP. To compare the GPU memory overhead among different methods, we visualize the amount of GPU memory requested by each method along the increase of task numbers during the training process. Specifically, we tracked the GPU memory usage of two groups of representative and challenging experimental scenarios: (1) Omniglot Rotation dataset with LeNet, which has 100 tasks in total; (2) TinyImageNet dataset with AlexNet, which has the largest number of parameters (i.e., #parameters ≈ 62 million, FLOPS ≈ 724 million in AlexNet) and the second largest number of tasks (i.e., 40 tasks). To make fair comparisons, we adopted the same hyperparameters (i.e., batch size, number of threads used in the data loader) for all the methods under each scenario, and moved all training-related operations (i.e., Singular Value Decomposition) onto the GPU devices. To monitor the GPU memory usage, we embedded some snippets with the Python package GPUutil (<https://pypi.org/project/GPUutil/>) into the training code. The amount of GPU memory requested during the training process is shown in the following Figure 7.

According to the visualization results in Figure 7, we can

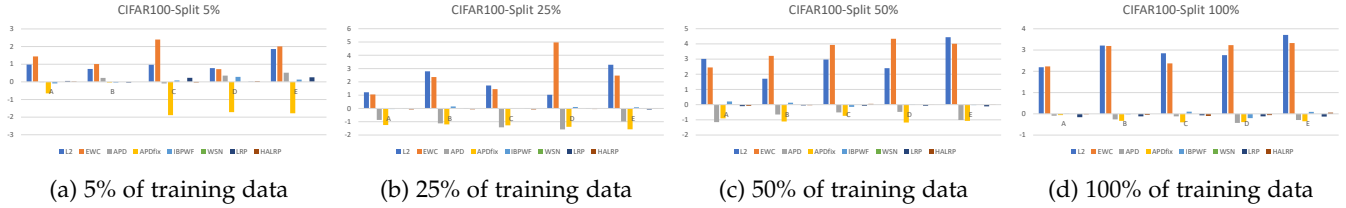


Fig. 5: Forgetting comparison on CIFAR100-Split with different task orders (A-E) under different amounts of training data.

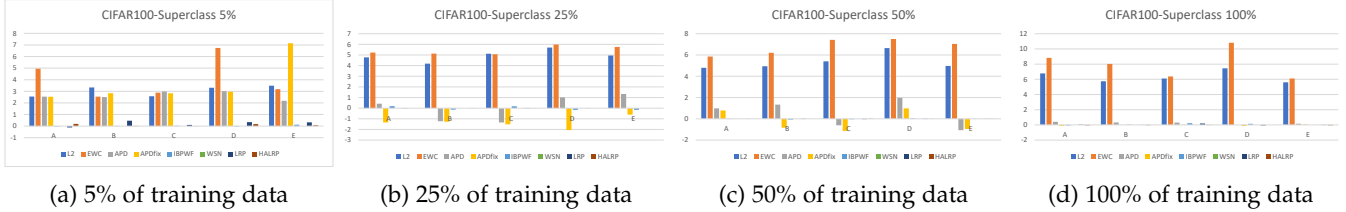


Fig. 6: Forgetting on CIFAR100-SuperClass with different task orders (A-E) under different amounts of training data.

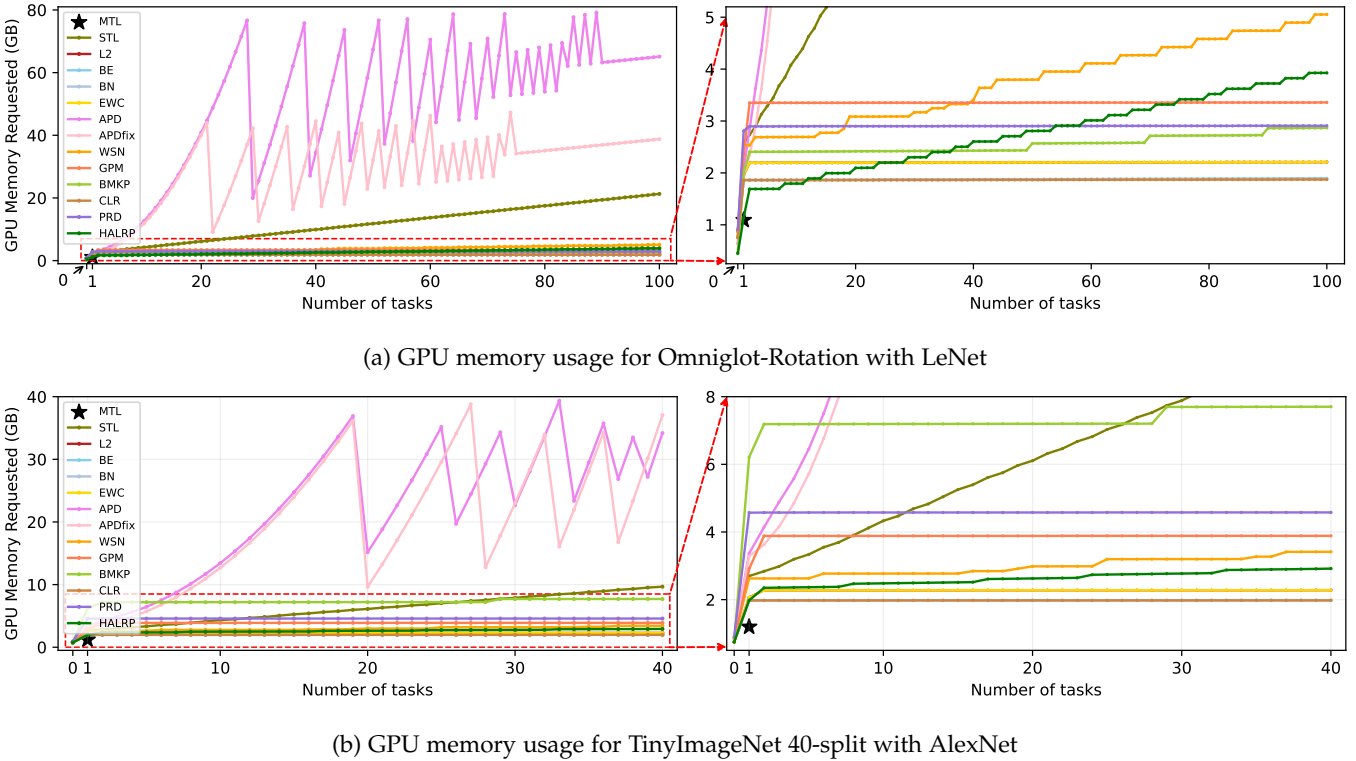


Fig. 7: Empirical statistics of GPU memory usage. The local zone with red rectangle in left is shown in the right plot.

observe that our proposed HALRP is still memory efficient compared to other baseline methods under these two challenging scenarios. Specifically, under the scenario for Omniglot Rotation datasets with LeNet (Fig. 7a, we can see that the amount of GPU memory requested by HALRP increased along the tasks but finally not exceeded 4GB for these 100 tasks. In contrast, APD and APDfix needed more GPU memory during training (i.e., maximum 80GB for APD and 45GB for APDfix), making the related experiments hard to be reproduced unless on some specific GPUs like NVIDIA A100 80G. As for TinyImageNet dataset with AlexNet, our proposed HALRP only requested about 3GB GPU memory

at the end of the 40-th task, which is much lower than APD and APDfix that needed at least 40GB memory during training, as well as BMKP that needs up to 8GB.

To summarize, our proposed method HALRP won't introduce heavy memory overhead. In the contrast, it is memory-efficient. The empirical results show that the requirement of training is easy to be satisfied and the scalability under the above challenging scenarios is easy to achieve.

APPENDIX F EXPERIMENTAL DETAILS

F.1 Dataset Preparation

CIFAR100 Splits/SuperClass We used the CIFAR100 Splits/SuperClass dataset following the evaluation protocol of [9], and follow the task order definition of [9] to test the algorithms with five different task orders (A-E).

For the CIFAR100 Split, the task orders are defined as:

- Order A: [0,1,2,3,4,5,6,7,8,9]
- Order B: [1, 7, 4, 5, 2, 0, 8, 6, 9, 3]
- Order C: [7, 0, 5, 1, 8, 4, 3, 6, 2, 9]
- Order D: [5, 8, 2, 9, 0, 4, 3, 7, 6, 1]
- Order E: [2, 9, 5, 4, 8, 0, 6, 1, 3, 7]

For the CIFAR100 SuperClass, the task orders are:

- Order A: [0, 1, 2, 3, 4, 5, 6, 7, 8, 9, 10, 11, 12, 13, 14, 15, 16, 17, 18, 19]
- Order B: [15, 12, 5, 9, 7, 16, 18, 17, 1, 0, 3, 8, 11, 14, 10, 6, 2, 4, 13, 19]
- Order C: [17, 1, 19, 18, 12, 7, 6, 0, 11, 15, 10, 5, 13, 3, 9, 16, 4, 14, 2, 8]
- Order D: [11, 9, 6, 5, 12, 4, 0, 10, 13, 7, 14, 3, 15, 16, 8, 1, 2, 19, 18, 17]
- Order E: [6, 14, 0, 11, 12, 17, 13, 4, 9, 1, 7, 19, 8, 10, 3, 15, 18, 5, 2, 16]

Furthermore, as discussed in the paper, we demonstrate the performance when handling limited training data. In this regard, we randomly select 5%, 25%, 50% training data from each task and report the corresponding accuracies.

P-MNIST We follow [19] to evaluate the algorithms' performance on the P-MNIST dataset. Each task of P-MNIST is a random permutation of the original MNIST pixel. We follow [19], [40] to generate the train/val/test splits and to create 10 sequential tasks using different permutations, and each task has 10 classes. We randomly generate five different task orders with five different seeds.

- seed 0: [6, 1, 9, 2, 7, 5, 8, 0, 3, 4]
- seed 1: [2, 9, 6, 4, 0, 3, 1, 7, 8, 5]
- seed 2: [4, 1, 5, 0, 7, 2, 3, 6, 9, 8]
- seed 3: [5, 4, 1, 2, 9, 6, 7, 0, 3, 8]
- seed 4: [3, 8, 4, 9, 2, 6, 0, 1, 5, 7]

Five dataset It uses a sequence of 5 different benchmarks including CIFAR10 [41], MNIST [42], notMNIST [43], FashionMNIST [44] and SVHN [45]. Each benchmark contains 10 classes. We follow [19] to generate the train/val/test splits and to create 10 sequential tasks using different permutations, and each task has 10 classes. We randomly generate five different task orders with five different seeds.

- seed 0: [2, 0, 1, 3, 4]
- seed 1: [1, 0, 4, 2, 3]
- seed 2: [2, 4, 1, 3, 0]
- seed 3: [3, 4, 1, 0, 2]
- seed 4: [0, 3, 1, 4, 2]

Omniglot-rotation We split this dataset [46] into 100 12-way classification tasks. We follow the train/val/test split of [19]. The five task order adopted in our experiments are:

- seed 0: [26, 86, 2, 55, 75, 93, 16, 73, 54, 95, 53, 92, 78, 13, 7, 30, 22, 24, 33, 8, 43, 62, 3, 71, 45, 48, 6, 99, 82, 76, 60, 80, 90, 68, 51, 27, 18, 56, 63, 74, 1, 61, 42, 41, 4, 15, 17, 40, 38, 5, 91, 59, 0, 34, 28, 50, 11, 35, 23, 52, 10, 31, 66, 57, 79, 85, 32, 84, 14, 89, 19, 29, 49, 97, 98, 69, 20, 94, 72, 77, 25, 37, 81, 46, 39, 65, 58, 12, 88, 70, 87, 36, 21, 83, 9, 96, 67, 64, 47, 44]
- seed 1: [80, 84, 33, 81, 93, 17, 36, 82, 69, 65, 92, 39, 56, 52, 51, 32, 31, 44, 78, 10, 2, 73, 97, 62, 19, 35, 94, 27, 46, 38, 67, 99, 54, 95, 88, 40, 48, 59, 23, 34, 86, 53, 77, 15, 83, 41, 45, 91, 26, 98, 43, 55, 24, 4, 58, 49, 21, 87, 3, 74, 30, 66, 70, 42, 47, 89, 8, 60, 0, 90, 57, 22, 61, 63, 7, 96, 13, 68, 85, 14, 29, 28, 11, 18, 20, 50, 25, 6, 71, 76, 1, 16, 64, 79, 5, 75, 9, 72, 12, 37]
- seed 2: [83, 30, 56, 24, 16, 23, 2, 27, 28, 13, 99, 92, 76, 14, 0, 21, 3, 29, 61, 79, 35, 11, 84, 44, 73, 5, 25, 77, 74, 62, 65, 1, 18, 48, 36, 78, 6, 89, 91, 10, 12, 53, 87, 54, 95, 32, 19, 26, 60, 55, 9, 96, 17, 59, 57, 41, 64, 45, 97, 8, 71, 94, 90, 98, 86, 80, 50, 52, 66, 88, 70, 46, 68, 69, 81, 58, 33, 38, 51, 42, 4, 67, 39, 37, 20, 31, 63, 47, 85, 93, 49, 34, 7, 75, 82, 43, 22, 72, 15, 40]
- seed 3: [93, 67, 6, 64, 96, 83, 98, 42, 25, 15, 77, 9, 71, 97, 34, 75, 82, 23, 59, 45, 73, 12, 8, 4, 79, 86, 17, 65, 47, 50, 30, 5, 13, 31, 88, 11, 58, 85, 32, 40, 16, 27, 35, 36, 92, 90, 78, 76, 68, 46, 53, 70, 80, 61, 18, 91, 57, 95, 54, 55, 28, 52, 84, 89, 49, 87, 37, 48, 33, 43, 7, 62, 99, 29, 69, 51, 1, 60, 63, 2, 66, 22, 81, 26, 14, 39, 44, 20, 38, 94, 10, 41, 74, 19, 21, 0, 72, 56, 3, 24]
- seed 4: [20, 10, 96, 16, 63, 24, 53, 97, 41, 47, 43, 2, 95, 26, 13, 37, 14, 29, 35, 54, 80, 4, 81, 76, 85, 60, 5, 70, 71, 19, 65, 62, 27, 75, 61, 78, 18, 88, 7, 39, 6, 77, 11, 59, 22, 94, 23, 12, 92, 25, 83, 48, 17, 68, 31, 34, 15, 51, 86, 82, 28, 64, 67, 33, 45, 42, 40, 32, 91, 74, 49, 8, 30, 99, 66, 56, 84, 73, 79, 21, 89, 0, 3, 52, 38, 44, 93, 36, 57, 90, 98, 58, 9, 50, 72, 87, 1, 69, 55, 46]

TinyImageNet This dataset contains 200 classes. In our experiments, we adopted two split settings: 20 split and 40 split.

Each task in the 20-split setting consists of 10 classes. We adopted five random tasks orders as follows:

- seed 0: [10, 18, 16, 14, 0, 17, 11, 2, 3, 9, 5, 7, 4, 19, 6, 15, 8, 1, 13, 12]
- seed 1: [11, 5, 17, 19, 9, 0, 16, 1, 15, 6, 10, 13, 14, 12, 7, 3, 8, 2, 18, 4]
- seed 2: [7, 6, 17, 8, 19, 15, 13, 0, 3, 9, 14, 4, 10, 12, 16, 5, 11, 18, 2, 1]
- seed 3: [8, 3, 6, 5, 15, 16, 2, 12, 0, 1, 13, 10, 19, 9, 14, 11, 4, 17, 18, 7]
- seed 4: [17, 19, 10, 14, 5, 18, 16, 11, 4, 8, 6, 0, 13, 1, 2, 15, 12, 3, 9, 7]

Each task in the 40-split setting consists of 5 classes. We adopted five random tasks orders as follows:

- seed 0: [22, 20, 25, 4, 10, 15, 28, 11, 18, 29, 27, 35, 37, 2, 39, 30, 34, 16, 36, 8, 13, 5, 17, 14, 33, 7, 32, 1, 26, 12, 31, 24, 6, 23, 21, 19, 9, 38, 3, 0]
- seed 1: [2, 31, 3, 21, 27, 29, 22, 39, 19, 26, 32, 17, 30, 36, 33, 28, 4, 14, 10, 35, 23, 24, 34, 20, 18, 25, 6, 13, 7, 38, 1, 16, 0, 15, 5, 11, 9, 8, 12, 37]

Dataset	CIFAR100 Split	CIFAR100 Super	PMNIST	Five dataset		Omniglot	TinyImageNet 40-split		TinyImageNet 20-split	
Network	LeNet	LeNet	LeNet	AlexNet	ResNet18	extended LeNet	AlexNet	ResNet18	AlexNet	ResNet18
n	20	20	12	12	12	20	50	50	50	50
n_r	1	1	1	1	3	1	20	25	25	25
α	0.9	0.9	0.9	0.9	0.95	0.99	0.9	0.9	0.9	0.9
LR	1e-3	1e-3	1e-3	1e-3	1e-3	5e-3	1e-3	5e-4	1e-3	5e-4
λ_0	1e-4	1e-4	1e-6	1e-6	1e-6	9e-5	5e-4	5e-4	1e-5	5e-4
λ_1	1e-4	1e-4	1e-3	1e-4	1e-4	1e-4	1e-4	1e-4	5e-4	1e-4
Bcsz	128	128	128	128	128	16	32	32	32	32

TABLE 8: Hyperparameters for the experiments. n : total epoch. n_r : warm-up epochs for a new task. LR: Learning rate. λ_0, λ_1 : coefficients for the regularization terms as discussed in Appendix D. Bcsz: training batch size.

- seed 2: [27, 9, 14, 0, 2, 30, 13, 36, 17, 37, 38, 29, 24, 12, 16, 1, 33, 23, 25, 19, 32, 10, 4, 6, 3, 34, 5, 28, 20, 26, 39, 21, 35, 31, 7, 11, 18, 22, 8, 15]
- seed 3: [29, 16, 9, 27, 4, 18, 28, 38, 15, 26, 25, 11, 30, 32, 13, 34, 39, 37, 5, 1, 31, 2, 22, 17, 14, 7, 12, 20, 36, 6, 23, 35, 33, 10, 19, 21, 0, 8, 3, 24]
- seed 4: [28, 39, 4, 15, 26, 20, 31, 7, 16, 11, 19, 33, 12, 18, 38, 13, 10, 22, 32, 25, 17, 36, 29, 14, 2, 24, 27, 6, 35, 34, 21, 37, 0, 3, 30, 9, 8, 23, 1, 5]

F.2 Model Architecture

In the experimental evaluations, we implement various kinds of backbone architectures to demonstrate our perturbation method for different deep models. We introduce the model architectures used in the paper

LeNet We implement two kinds of LeNet models: **1)** For CIFAR100 Splits/SuperClass and P-MNIST, we implement the general LeNet model with neurons 20-20-50-800-500. **2)** For Omniglot-Rotation, we follow [9], [19] to implement the enlarged LeNet model with neurons 64-128-2500-1500.

AlexNet For the experiments on Five-dataset and TinyImageNet, we implement AlexNet model by following [2], [19].

ResNet-18 We adopted the reduced ResNet-18 model (i.e., reduce half of the filters in each convolutional layer from the standard Resnet18) on the Five-dataset and TinyImageNet by following [19].

F.3 Training Hyperparameters

We reimplement the baselines by rigorously following the official code release or publicly accessible implementations and tested our proposed algorithm with a unified test-bed with the same hyperparameters to get fair comparison results. The training details for our experiments are illustrated in Table 8. The hyperparameters are selected via grid search. We also provide descriptions of the hyperparameters in the source code.